Finding water scarcity amid abundance using human–natural system models

William K. Jaeger[a,1], Adell Amos[b], Daniel P. Bigelow[c], Heejun Chang[d], David R. Conklin[e], Roy Haggerty[f], Christian Langpap[a], Kathleen Moore[a], Philip W. Mote[g], Anne W. Nolin[h], Andrew J. Plantinga[i], Cynthia L. Schwartz[j], Desiree Tullos[j], and David P. Turner[k]

[a]Department of Applied Economics, Oregon State University, Corvallis, OR 97331; [b]School of Law, University of Oregon, Eugene, OR 97403; [c]Economic Research Service, US Department of Agriculture, Washington, DC 20024; [d]Department of Geography, Portland State University, Portland, OR 97201; [e]Oregon Freshwater Simulations, Portland, OR 97213; [f]College of Science, Oregon State University, Corvallis, OR 97331; [g]Oregon Climate Change Research Institute, Oregon State University, Corvallis, OR 97331; [h]College of Earth, Ocean, and Atmospheric Sciences, Oregon State University, Corvallis, OR 97331; [i]Bren School of Environmental Science and Management, University of California, Santa Barbara, CA 93106; [j]Biological and Ecological Engineering Department, Oregon State University, Corvallis, OR 97331; and [k]Forest Ecosystems and Society, Oregon State University, Corvallis, OR 97331

Edited by Jacob Schewe, Potsdam Institute for Climate Impact Research, Potsdam, Germany, and accepted by Editorial Board Member Hans J. Schellnhuber September 20, 2017 (received for review April 25, 2017)

Water scarcity afflicts societies worldwide. Anticipating water shortages is vital because of water's indispensable role in social-ecological systems. But the challenge is daunting due to heterogeneity, feedbacks, and water's spatial-temporal sequencing throughout such systems. Regional system models with sufficient detail can help address this challenge. In our study, a detailed coupled human–natural system model of one such region identifies how climate change and socioeconomic growth will alter the availability and use of water in coming decades. Results demonstrate how water scarcity varies greatly across small distances and brief time periods, even in basins where water may be relatively abundant overall. Some of these results were unexpected and may appear counterintuitive to some observers. Key determinants of water scarcity are found to be the cost of transporting and storing water, society's institutions that circumscribe human choices, and the opportunity cost of water when alternative uses compete.

water scarcity | climate change | coupled human–natural system | hydro-economic model | conveyance cost

Declining access to water is a significant problem for up to 2 billion people, impairing food production, human health, economic development, and ecosystem services (1). Water scarcity can result in crop failures, wildfire, fish die-offs, urban water shutoffs, and groundwater depletion leading to irreversible land subsidence (2). Contributing factors include growing populations, incomes, and a changing climate. Recent droughts in the western United States have resulted in substantial losses to agriculture and other sectors, and damages to forests, fish, and wildlife (3, 4).

Water is an integral part of social-ecological systems. Predicting water scarcity and designing mitigation and adaption policies can be extremely challenging because these systems are complex and are characterized by nonlinear feedbacks, strategic interactions, and social, spatial, and temporal heterogeneity (5).

Previous studies have investigated water scarcity at regional or national scales using aggregate measures of water abundance relative to overall demand (6, 7). Supply has typically been measured as annual basin discharge, and demand projections have reflected average per capita water use (7, 8). Given the complex role water plays in human–natural systems, such aggregate approaches may not be able to anticipate when and where water scarcity may emerge, making it difficult for policymakers to address rising water scarcity.

This study examines how climate change, population growth, and economic growth will alter the availability and use of water in coming decades, using the example of the Willamette River Basin (WRB), Oregon. The model developed for this purpose has high spatial and temporal resolution, and detailed representations of economic and biophysical subsystems (see *SI Appendix* for details). Models of coupled human–natural systems take many forms (5, 9). Where markets and incentives partly drive allocation and use of land, water and other resources have been integrated in human process and biophysical models in a simulation or optimization framework (e.g., refs. 10 and 11) including climate-economy models (12). The main components and linkages of this model are characterized in Fig. 1, indicating how human uses of land and water interact with flows of surface and groundwater, mediated by water rights, markets, and regulations. The goals of the study are twofold: first, to understand where and when water scarcity may arise and to recognize the factors contributing to, and potentially mitigating, future water scarcity; and second, to assess the importance of a high level of system detail to gain insights into emerging water scarcity.

The results are illuminating in two main ways. First, the model reveals unexpected changes in water availability and use arising from interactions between human and natural subsystems. In some cases, feedbacks or indirect effects in one component of the model offset expected direct scarcity impacts. Second, the model demonstrates that water scarcity, defined as the marginal value of a unit of water (13), varies significantly across small distances (meters) and brief time periods (days), even in our study basin, where water is relatively abundant overall. There are three key contributors to water scarcity: (*i*) the costs of transporting water across locations, storing water over time, and transforming the quality

Significance

Climate change will heighten the need to anticipate water shortages worldwide. The task is daunting due to water's variability, spatial-temporal movement, feedbacks, and other system complexities. A high-resolution coupled human–natural system model identifies how both climate change and socioeconomic drivers will alter water scarcity in future decades. The results illuminate how water scarcity varies greatly across small distances and brief time periods, even in basins where water may be relatively abundant overall. These findings, and other unexpected results that may seem counterintuitive, underscore the potential value of such models for policy.

Author contributions: W.K.J., A.A., D.P.B., H.C., D.R.C., R.H., C.L., K.M., P.W.M., A.W.N., A.J.P., C.L.S., D.T., and D.P.T. designed research, performed research, analyzed data, and wrote the paper.

The authors declare no conflict of interest.

This article is a PNAS Direct Submission. J.S. is a guest editor invited by the Editorial Board.

Data deposition: The data reported in this paper have been deposited in ScholarsArchive@OSU: hdl.handle.net/1957/58613, hdl.handle.net/1957/58612, hdl.handle.net/1957/59984, hdl.handle.net/1957/59886, and hdl.handle.net/1957/48884.

[1]To whom correspondence should be addressed. Email: wjaeger@oregonstate.edu.

This article contains supporting information online at www.pnas.org/lookup/suppl/doi:10.1073/pnas.1706847114/-/DCSupplemental.

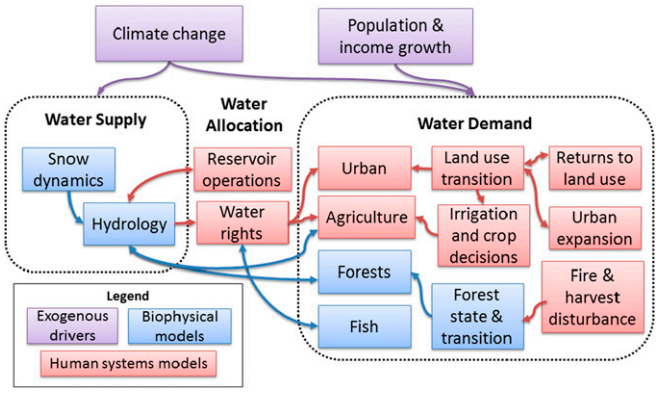

Fig. 1. Diagram of WRB model components and linkages.

of water (e.g., temperature, salinity); (*ii*) the effectiveness of institutions in allocating water, including property rights, regulations, and other governance mechanisms that impact water use (14); and (*iii*) the opportunity cost of water, when one use for water competes with other, possibly more valuable, uses. These economic and institutional factors are key to explaining how scarcity can coexist with overall abundance.

Modeling the WRB, Oregon

The WRB faces water scarcity due to declining snowpack, population growth, rising demands from agriculture, and the effects of warmer air temperatures on forest health, wildfires, river temperatures, and endangered fish. The WRB covers 29,728 km^2, ~12% of Oregon's land area. The Willamette River—a major tributary of the Columbia River—is the 19th largest river in the United States. Its mainstem is 301 km long, flowing north between the Oregon Coast and Cascade Ranges. The WRB is home to over 70% of the state's population of nearly 4 million. Two-thirds of the basin's population is concentrated in the Portland Metro area (Fig. 2*A*).

The basin's hydrology is notable for the mismatch between winter inflows and summer demand. The valley is prone to flooding from November to March due to precipitation on saturated soils, atmospheric rivers, and snowmelt (15), whereas streamflows are lowest during the dry summer farming season.

The Willamette Valley is one of the most fertile agricultural regions in North America, with about 1.5 million acres of farmland, 30% of which has irrigation water rights. Human uses of water are governed under western US water law by a seniority system, environmental regulations, and public infrastructure, including 13 federal dams constructed for flood mitigation but also providing hydropower, storage, and recreation. In addition, large instream flows are protected for navigation, pollution abatement, recreation, and aquatic habitat.

The Model. We developed a hydroeconomic process model of the basin's major human and natural systems with high spatial resolution (160,000 polygons averaging 18.6 ha in size) and daily to annual timescales from 2010 to 2100 (Fig. 1). Exogenous elements include daily meteorology (temperature, precipitation, humidity, wind, radiation) for three representative climate change scenarios derived from regional climate data downscaled to 4-km resolution (16–18), and annual population and income projections.

Annually modeled processes include spatially explicit forest growth, harvest and wildfires (19), endogenous land values and land-use changes (predicted using empirically based functions adapted from refs. 20 and 21, respectively), endogenous regulatory adjustments to urban growth boundaries (similar to ref. 20), water rights, crop choices, and irrigation decisions (22). Daily modeled processes include spatially referenced routing of surface hydrology based on algorithms developed by Bergström and others (23, 24). Snow accumulation and ablation uses a modified version of the Hydrologiska Byråns Vattenbalansavdelning (HBV) degree-day model of Seibert (25). Evapotranspiration of forests (described in

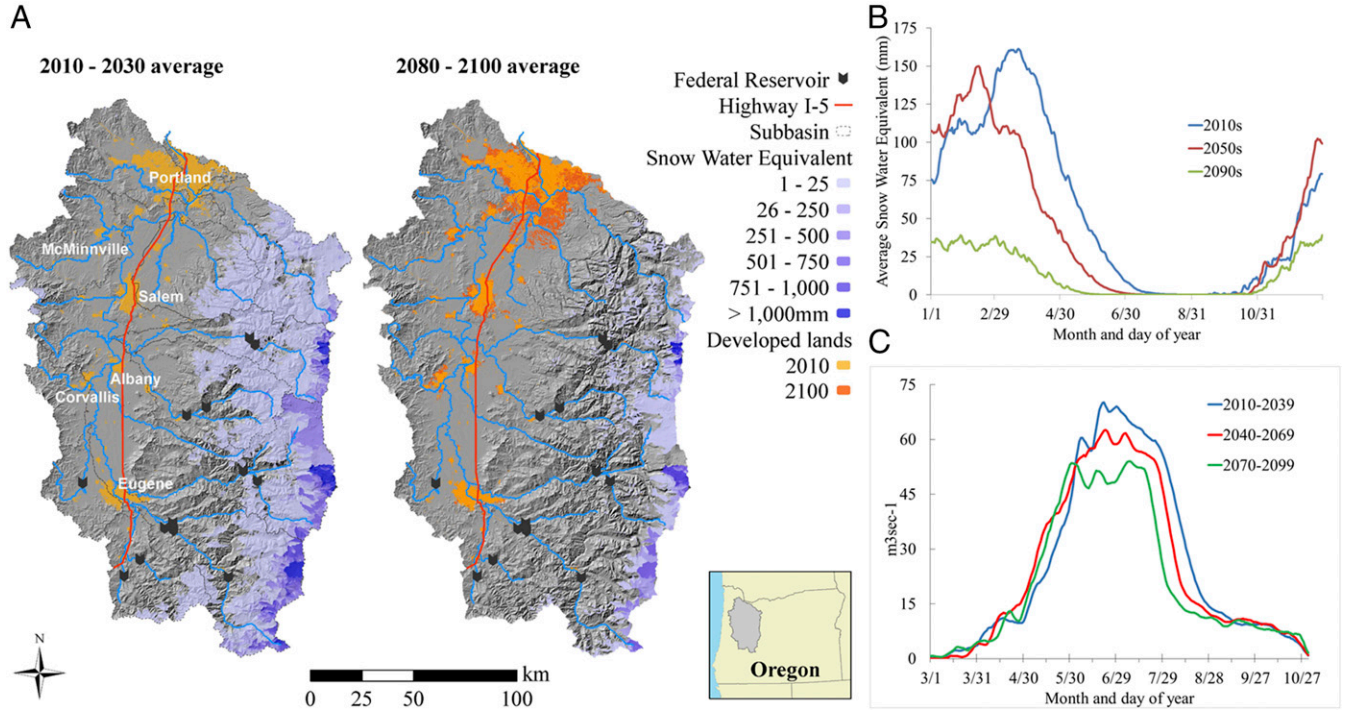

Fig. 2. Projected changes in the WRB 2010–2100: developed land use and April 1 average snowpack (snow–water equivalent, SWE) (*A*); projected seasonal average snow accumulation and melt in future decades (*B*); and projected changes in levels and timing of irrigation diversions (*C*).

ref. 26) adapted the Penman–Monteith approach. Spatially explicit irrigation and municipal water rights were fully represented. Crop planting, growth, and daily evapotranspiration were modeled following FAO-56 (27, 28) and similar to Seibert (29). Additionally, soil moisture, groundwater flows, economic models of farm irrigation decisions and urban water use, as well as the releases from 13 federal dams, were developed for this study. See *SI Appendix* for detailed descriptions.

These submodels are linked using *Willamette Envision*, an integrated modeling framework that simulates spatially and temporally explicit human and natural system processes, as described in *SI Appendix*. The reference case and alternative scenarios were developed working closely with a broad stakeholder community.

Reference Case Scenario. The central simulation is a "reference case" scenario that reflects midrange projections for climate change and population and income growth, as well as status quo assumptions for most institutions (water rights, land use regulations, reservoir and forest management), for technology, and for most prices. Over 20 alternative scenarios were simulated for sensitivity analysis (e.g., high climate change, high population growth), counterfactual comparisons to isolate specific changes (no population growth, stable climate), to evaluate policies to mitigate future water scarcity (irrigation expansion, high water prices), or as combinations. See *SI Appendix* for details.

The reference case scenario finds that annual outflow from the Willamette River averages 29.6×10^9 m^3 [24×10^6 acre-feet (af)], whereas human withdrawals plus instream regulatory flows average 5.5×10^9 m^3 (4.5×10^6 af). This apparent surplus would appear to preclude water scarcity. Nevertheless, notable scarcity emerges when we examine finer spatial and temporal scales.

Based on over 40 climate scenarios, the downscaled general circulation model (GCM)-derived outputs indicate that by the year 2100, the WRB will be between 1.1 °C (2 °F) and 7 °C (12.6 °F) warmer than today (19, 20). Winter temperatures are projected to rise between 0.5 °C (33 °F) and 5.5 °C (42 °F). The months of July to September are projected to warm about 2 °C (3.6 °F) more than in winter. Climate models differ about whether the WRB will be drier or wetter, but the majority of climate model runs examined show slightly wetter winters and drier summers.

Population is projected to increase from 2.6 million to 5.4 million over the period (*SI Appendix*, Table S1), expanding developed land area by 53% (716 km^2) and displacing 469 km^2 previously in agriculture and 235 km^2 previously in forest use (Fig. 2*A*). Urban water use is projected to rise by 110%, due mainly to population growth. Real household income is expected to increase by 175% by 2100.

Snowpack, in the midrange climate scenarios, declines between 87% and 94% by 2100 (Fig. 2 *A* and *B*), hastening runoff and reducing spring and summer flows. In subbasins without reservoirs or with low groundwater contributions, these changes reduce the water available at lower elevations. In particular, the federal reservoirs fill to lower levels during the summer when reservoir recreation competes with "minimum conservation flows" established under the US Endangered Species Act (ESA) (30) and other obligations, including irrigation water rights tied to stored water.

Variations Across Subbasins. Snow provides winter storage and spring-summer flows for higher elevation eastern subbasins, but very little for lower elevation western subbasins (Fig. 2*A*). Even among eastern subbasins, the impact of snow on streamflow varies substantially due to differences in elevation and geologic mediation of low flows by groundwater contributions (15, 31). These differences are reflected in Table 1 (columns A and B), where the April–September flux varies by a factor of eight. The adequacy of existing flows to meet regulatory minimums also varies by subbasin (Table 1, columns C and D). Moreover, April–August flows in some subbasins decline relative to instream requirements (column E).

Some of the differences affecting water scarcity across subbasins are due to changes in urban and agriculture land uses (columns F–H), differences in forest growth due to harvest and wildfires, and differences in how land cover changes affect snow and runoff due to evapotranspiration and snow sublimation. For example, forest harvest and wildfires can cause large changes in forest water use (discussed below).

Finding Scarcity Amid Abundance

The Role of Costs. If it were costless to store and transport water, or to improve its quality, water scarcity could in principle be eliminated given the overall abundance of water in the WRB (barring institutional impediments). Our analysis, however, indicates that water scarcity in the WRB varies seasonally and across locations and uses. Relatively fine-scale processes such as market adjustments, barriers due to costs and profitability, or government regulations can have large consequences for scarcity.

Water storage and transportation costs are not uniform across the WRB. In some cases, these costs are very low, as with gravity-based conveyance in summer along watercourses below federal reservoirs. Although built primarily for flood regulation, in summer the reservoirs normally store 2×10^9 m^3 (1.6×10^6 af) of water, much of which could be released to flow downstream at

Table 1. Differences in hydrology and economics across subbasins

River Basin	Avg. flow April-Sept, m^3/s (A)	Flow April-Sept, mm/d (B)	Regulatory min. April-Sept, m^3/s (C)	Avg. flow/reg. min., July-Aug. (D)	Change in April-Aug. flow 2010–20s to 2080–90s, % (E)	Farmland , % of area (F)	Surface irrigation, % of basin (G)	Developed land, % of land area (H)
Clackamas	64	2.3	14.7	2.8	–4.1	7.9	0.5	1.7
Long Tom*	8	0.7	0.8	2.1	8.0	29.9	4.3	6.5
Marys*	9	1.0	1.8	1.5	13.5	22.9	2.7	2.9
McKenzie	107	2.7	29.0	2.4	–7.3	2.0	0.4	0.5
Molalla	42	1.6	9.2	2.7	–0.5	39.0	4.8	3.2
North Santiam	128	5.6	36.8	2.3	–3.9	9.9	1.6	0.5
South Santiam	66	2.1	30.2	1.3	–1.4	14.8	2.5	0.6
Tualatin River*	21	1.0	4.4	1.6	17.0	28.4	6.3	18.2
Yamhill River*	18	1.2	0.9	1.7	11.3	54.6	12.1	3.8
Willamette, Coast & Middle Forks	88	1.5	61.4	0.7	–3.4	3.4	0.4	0.5
Average	55	2	19	1.9	2.9	23.3	3.9	4.2

*Indicates subbasins on the western side of the WRB (Fig. 3).

negligible cost. Most farmland, however, is not adjacent to watercourses downstream of federal dams. Farmers invest in new irrigation if it is profitable—if the additional cost of transporting reservoir-released surface flows to currently unirrigated farmland is less than the added revenue from irrigating. For each of the 405,000 ha (1×10^6 ac) currently without irrigation water rights, both the added conveyance costs and increased revenue were estimated (*SI Appendix*, section 5.4.5). When farmers were allowed to adopt new irrigation from stored water in an alternative scenario, it was found to be profitable on only about 3,240 ha (8,000 ac) due to the high water conveyance costs. Even when the costs are assumed to be optimistically low, less than 11,130 ha (28,000 ac) adopt irrigation.

One example of rising water scarcity in the WRB pertains to forests, where climate change is increasing moisture stress and threatening forest health (32). As the climate warms, rising air temperatures increase atmospheric evaporative demand and forest evapotranspiration (ET). In mid- to late summer, however, soil water limits ET so that warmer temperatures, when combined with less snow, lead to a longer summer dry period. Given the prohibitive cost of transporting water from reservoirs to forests, the anticipated result is increased water scarcity resulting in a 200–900% increase in forest wildfires across the three climate scenarios (26). The likely outcome will be increased costs for fire suppression, the transition to new forest types, and reduced availability of forestland for timber harvest (26) (*SI Appendix*, section 4.2).

The Role of Water Rights and Other Institutions. Water rights and other federal, state, and local regulations play a critical role in determining where, when, and for what uses water may be scarce (14). Surface water "live flow" rights were fully appropriated in the WRB by the 1990s, meaning that farms without these rights have no access to surface water for irrigation. Under western US water law, the amounts, timing, and uses of water rights are limited, and yearly fluctuations in supply lead to allocations based on a seniority system that can "shutoff" deliveries for relatively junior water rights (33). Indeed, the scarcity created by irrigation water rights is one key factor that produces a 10-fold variation in agricultural land values in the basin (Fig. 3 and *SI Appendix*, Fig. S3).

Instream flows, however, represent by far the largest societal allocation of water in the WRB. State and federal laws protect instream flows for navigation, pollution abatement, recreation, and aquatic habitat. Perennial minimum streamflows were established in the 1960s, although a fraction of these have yet to be implemented as instream water rights (33). Indeed, when the remaining ("unconverted") perennial minimum streamflows are implemented, they will add 1.35×10^9 m^3 to minimum outflows from the 11 major tributaries that join the mainstem Willamette River (based on model results).

Federal laws also have a substantial influence on water allocation in the WRB. Minimum flows are mandated under the ESA, in turn prompting targeted releases from federal reservoirs. These federal laws interact in complex ways with state law (33). Indeed, current ESA-related requirements for April–October minimum flows have led regulators to cap stored water irrigation contracts at 6% of the total stored volume (30) (a nonbinding limit in our model).

Differentiation Across Space, Time, and Use. Analyses at the basin or national scale, such as global assessments of the impacts of climate change and population growth on future water shortages (8, 34–37), will be unable to detect these kinds of causal relationships that produce localized scarcity. For example, the 2×10^9 m^3 of water stored each summer would appear to be an ample source for the 405,000 ha of currently nonirrigable farmland (indeed this water is currently "reserved" for agriculture under federal law), but the cost of conveyance makes this economically prohibitive. Within the basin, the scarcity contrasts are stark. In some areas, farmers have abandoned water rights or use them intermittently, suggesting low marginal value of water. In the Pudding River basin, by contrast, conflict has emerged over a proposed $60 million reservoir that would permanently flood some farmland to ensure irrigation water for other farmers. The conflict is emblematic of the complex ways that economics and institutions interact: Increased instream flows for three endangered fish, combined with declining groundwater, have led one group of irrigators on high-value land with low-priority irrigation water rights to enlist an extraordinary legal tool (eminent domain) to gain approval for a storage reservoir that will inundate other, relatively low-value farmland (38).

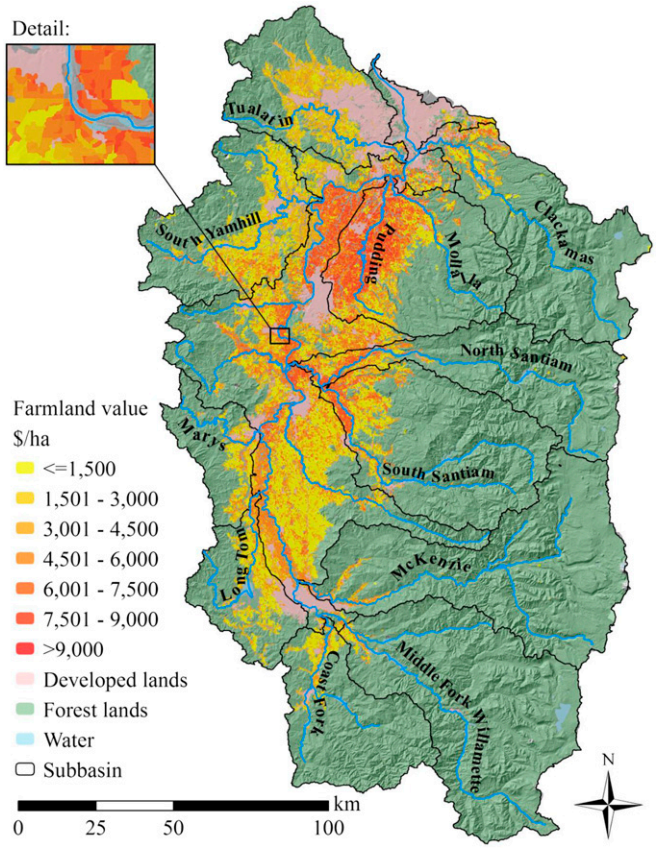

Fig. 3. Variation in agricultural land values; subbasin locations.

That scarcity can exist amid aggregate abundance is not unique to water. Indeed, in the case of food, for example, Sen (39) showed that major famines were not generally the result of an aggregate shortage of food. Sen found large differences among households in their ability to acquire food, due to differences in economic and institutional factors including costs, market conditions, rights of ownership, and exchange. These factors are analogous to the cost, profitability, water rights, and other institutions identified here in the case of water in the WRB.

The Challenge of Predicting Future Water Scarcity

The dynamics of water demand and supply in regional systems have the potential to generate unexpected outcomes, often arising from the linkages and feedbacks between system components. In the WRB, expanded urban development will displace agriculture and forests, but also increase the magnitude of potential flood damages, which could alter the optimal timing of reservoir refill (40). A warmer climate melts snowpack earlier, increases wildfires, affects vegetation and ET; encourages earlier planting and irrigation; and possibly changes crop choice. Additionally, instream

minimum flow requirements aimed at protecting ecosystem services will increase competition with out-of-stream demands (33).

System linkages and feedbacks can be highly idiosyncratic across subbasins and vary at fine spatial and temporal scales. Without a model, it would have been extremely difficult to identify and predict these relationships for the WRB. Three examples illustrate the challenges that such dynamics represent for predicting water scarcity and designing policy responses.

Offsetting Seasonal Shifts in Supply and Demand. In the first example, climate warming generates two responses, one in water supply and one in demand. The first response to warmer temperatures is a reduction in snow accumulation and melt, along with a shift in melt timing to earlier in spring. This response reduces summer surface flows. The second response is a human response. Because of warmer spring temperatures, farmers are able to plant earlier, which shifts both the start and the completion of irrigation (Fig. 2*C*). Thus, a larger proportion of irrigation occurs earlier in the year, when snowmelt runoff and precipitation are higher. This decreases the projected number of irrigation shutoffs due to water scarcity by 10–30% in both the reference case and high climate change scenarios. This is because, although in future decades surface water supplies become relatively scarce in late July and August, irrigators have increasingly completed irrigating by that time, resulting in fewer regulatory shutoffs.

The shift to earlier planting dates has an additional positive effect on water scarcity: Although warmer midsummer temperatures would generally raise crop ET and increase irrigation requirements, the earlier planting has an offsetting effect. More of the plant's growth takes place when temperatures are lower and precipitation is higher, resulting in no rise in average crop ET during the 90-y simulation.

Urban Demand Growth and Reduced Irrigation. The second example involves the potential mitigating effect of urban growth on water scarcity. Projected growth in urban water demand is the single largest change in direct human water use through 2100. Many city governments in the basin face uncertainty about how best to secure adequate future water supplies. Surface flows are already fully appropriated, and rights to federally stored water are reserved for agriculture. Moreover, instream flow requirements account for a majority of summer water allocations. However, a city's growing demand for water will coincide with urban land expansion, and the likely patterns of this expansion overlap with some of the spatially referenced irrigation water rights in our model. For the six main metropolitan areas, the model predicts urban consumptive use of water (from outdoor use only since indoor water use is returned to streams with minor losses) to increase 45×10^6 m^3 (Table 2). However, due to the land use changes accompanying this growth, the displacement of surface irrigation offsets one-third of the increase. These effects vary significantly across cities depending on the extent and direction of urban expansion and on the proximity to surface irrigated farmlands. When groundwater irrigation is included, more than 80% of the urban water use increases are offset by reduced irrigation in our model (Table 2).

Forest Water Use and Wildfire. The third example involves climate change and forest water use. With warmer temperatures, water requirements for a given stand of forest will increase, but drier forests are also more prone to wildfires. Increases in wildfire frequency will result in a more open and patchy landscape with fewer mature trees and, thus, a lower average foliage density (leaf area) (19). Because forest water use (ET and canopy snow sublimation) varies positively with leaf area, more wildfires mean a reduction in water use. This, in turn, allows more precipitation falling in forest zones to be routed downstream. This means that climate change could actually lead to increases in the runoff ratio despite increasing evaporative demand (26). In our reference case scenario, there is a projected decrease in forest water use of 315 million m^3 for April–July between the 2010s and 2090s due mainly to the effects of projected wildfires (*SI Appendix*, section 4.2). Efforts to suppress wildfires can be expected to increase forest water use. Indeed, a counterfactual scenario that represents the high climate scenario but with no wildfires finds increased forest water use by 1.4 billion $m^3 \cdot y^{-1}$. While subbasin-specific impacts from wildfire are impossible to predict since the location of future wildfires is unknown, this example illustrates the possibility of unexpected results that may appear counterintuitive.

Fine Scale and Large Magnitudes. In addition to these examples of how feedbacks and linkages can produce unexpected results, we find a strikingly high variability in water scarcity at fine spatial and temporal scales. For example, upland forested areas will exhibit high water stress and increased wildfire risk (*SI Appendix*, section 4.2), despite in some cases being close to large federal reservoirs. Similarly, distances as small as 100 m separate irrigators whose legal right to water exceeds what can be put to beneficial use from farmers who have no economically feasible options to acquire irrigation water rights, due to protected instream flows or high conveyance costs that make more distant options uneconomical.

Another powerful way in which this type of model is valuable is that it compels us to recognize what is large versus what is small. Many components related to water supply or demand turn out to be much larger (or smaller) than initially believed. For example, initially Willamette Water 2100 researchers and stakeholders focused on future urban industrial water and did not pay attention to forest water use, but the former has turned out to be nearly negligible relative to the latter. Similarly, the anticipated expansion in crop irrigation in the basin has been a central rationale for reserving the water stored in federal reservoirs for agriculture. However, we find that only 1–3% of unirrigated land would be able to bring stored surface water into use profitably, due to the high transport costs.

Using Regional System Models for Water Policy

Water shortages frequently come with high social costs. The annual costs of California's recent experience have been estimated

Table 2. Urban water demand growth net of displaced irrigation, 2010–2100 (1,000 m^3)

		Net of displaced irrigation:	
Urban area	Change in urban water use	Surface only	Surface and groundwater
Portland	30,872	21,626	7,195
McMinnville	1,457	−819	−1,528
Salem	7,391	4,616	989
Albany	1,510	1,208	393
Corvallis	1,004	486	−155
Eugene	3,158	2,513	618
Total	45,392	29,629	7,512

at $2–3 billion (41). Whether shortages are the result of short-term drought conditions, the cumulative impacts of decades of misguided water policies, or long-term shifts in water supply and demand, the costs are high, and hence so too are the potential benefits from intervening to mitigate future water crises. A system model can be a critical tool for designing effective policy interventions. The value of a given model will depend on whether it sheds new light on critical factors or key processes, and whether this new information is heeded by policymakers. In the case of the WRB, the model has allayed some fears (urban water shortages), while shifting focus toward other, less easily remedied sources of scarcity (forest health, instream flows, and stream temperatures).

Many of the insights from this model have clear relevance, applicability, and implications for other basins. For example, elsewhere in the western United States, emerging water scarcity can also be expected to exhibit high spatial and temporal specificity, even while the particular causes and potential solutions may differ. In California, for example, rather than wildfires reducing water use by forests, climate change may cause changes in vegetation that increase forest consumptive use (42). Models of this kind may be particularly valuable in basins such as the Indus or Nile, where climate change, population growth, poverty and institutional failures place large vulnerable populations at high risk.

ACKNOWLEDGMENTS. This project was supported by National Science Foundation Grants 1039192 (Oregon State University), 1038925 (Portland State University), and 1038899 (University of Oregon). More detailed data descriptions are found at inr.oregonstate.edu/ww2100/data. The views expressed are those of the authors and do not reflect those of the US Department of Agriculture or Economic Research Service.

1. Millennium Ecosystem Assessment (2005) *Ecosystems and Human Well-Being: Wetlands and Water. Synthesis* (World Resour Institute, Washington, DC).
2. Watkins K (2006) Human Development Report 2006-beyond scarcity: Power, poverty and the global water crisis. UNDP Human Development Report (Palgrave Macmillan, New York).
3. MacDonald GM (2010) Climate change and water in Southwestern North America special feature: Water, climate change, and sustainability in the southwest. *Proc Natl Acad Sci USA* 107:21256–21262.
4. AghaKouchak A, Feldman D, Hoerling M, Huxman T, Lund J (2015) Water and climate: Recognize anthropogenic drought. *Nature* 524:409–411.
5. Levin S, et al. (2013) Social-ecological systems as complex adaptive systems: Modeling and policy implications. *Environ Dev Econ* 18:111–132.
6. Hoekstra AY, Mekonnen MM, Chapagain AK, Mathews RE, Richter BD (2012) Global monthly water scarcity: Blue water footprints versus blue water availability. *PLoS One* 7:e32688.
7. Schewe J, et al. (2014) Multimodel assessment of water scarcity under climate change. *Proc Natl Acad Sci USA* 111:3245–3250.
8. Vörösmarty CJ, Green P, Salisbury J, Lammers RB (2000) Global water resources: Vulnerability from climate change and population growth. *Science* 289:284–288.
9. Cai X, McKinney DC, Lasdon LS (2003) Integrated hydrologic-agronomic-economic model for river basin management. *J Water Resour Plan Manage* 129:4–17.
10. Bateman IJ, et al. (2013) Bringing ecosystem services into economic decision-making: Land use in the United Kingdom. *Science* 341:45–50.
11. Rabotyagov SS, et al. (2014) Cost-effective targeting of conservation investments to reduce the northern Gulf of Mexico hypoxic zone. *Proc Natl Acad Sci USA* 111: 18530–18535.
12. Intergovernmental Panel on Climate Change (2014) *Climate Change 2014–Impacts, Adaptation and Vulnerability: Regional Aspects* (Cambridge Univ Press, New York).
13. Jaeger WK, et al. (2013) Toward a formal definition of water scarcity in natural-human systems. *Water Resour Res* 49:4506–4517.
14. Jaeger WK (2015) *"Institutions and Water" in Handbook of Water Economics*, eds Dinar A, Schwabe K (Edward Elgar Publishing, Northhampton, MA).
15. Chang H, Jung I-W (2010) Spatial and temporal changes in runoff caused by climate change in a complex large river basin in Oregon. *J Hydrol (Amst)* 388:186–207.
16. Rupp DE, Abatzoglou JT, Hegewisch KC, Mote PW (2013) Evaluation of CMIP5 20th century climate simulations for the Pacific Northwest USA. *J Geophys Res Atmos* 118: 10884–10906.
17. Vano JA, Kim JB, Rupp DE, Mote PW (2016) Selecting climate change scenarios using impact-relevant sensitivities. *Geophys Res Lett* 42:5516–5525.
18. Abatzoglou JT (2012) Development of gridded surface meteorological data for ecological applications and modelling. *Int J Climatol* 33:121–131.
19. Turner DP, Conklin DR, Bolte JP (2015) Projected climate change impacts on forest land cover and land use over the Willamette River Basin, Oregon, USA. *Clim Change* 133:335–348.
20. Bigelow DP, Plantinga AJ, Lewis DJ, Langpap C (2017) How does urbanization affect water withdrawals? Insights from an econometric-based landscape simulation. *Land Econ* 93:413–436.
21. Lewis DJ, Plantinga AJ, Nelson E, Polasky S (2011) The efficiency of voluntary incentive policies for preventing biodiversity loss. *Resour Energy Econ* 33:192–211.
22. Kalinin A (2013) *Right as Rain?: The Value of Water in Willamette Valley Agriculture* (Oregon State University, Corvallis, OR).
23. Bergström S (1995) The HBV model. *Computer Models of Watershed Hydrology*, ed Singh VP (Water Resources Publications, Denver), pp 443–476.
24. Bergström S, et al. (2001) Climate change impacts on runoff in Sweden assessments by global climate models, dynamical downscaling and hydrological modelling. *Clim Res* 16:101–112.
25. Seibert J (1997) Estimation of parameter uncertainty in the HBV model. *Nord Hydrol* 28:247–262.
26. Turner DP, et al. (2016) Assessing mechanisms of climate change impact on the upland forest water balance of the Willamette River Basin, Oregon. *Ecohydrology* 16: 2345–2355.
27. Allen RG, Pereira LS, Raes D, Smith M (1998) Crop evapotranspiration-guidelines for computing crop water requirements-FAO irrigation and drainage paper 56. *FAO Rome* 300:6541.
28. Allen RG, Robison CW (2007) *Evapotranspiration and Consumptive Irrigation Water Requirements for Idaho* (University of Idaho Research and Extension, Kimberly, Idaho).
29. Seibert J (2005) HBV-Light (Stockholm). Available at people.su.se/~jseib/HBV/HBV_light.html. Accessed March 5, 2015.
30. NOAA (National Oceanic & Atmospheric Administration) (2008) Consultation on the "Willamette River Basin flood control project" (NOAA National Marine Fisheries Service, Northwest Region, Seattle), NOAA Fisheries Log No. F/NWR/2000/02117.
31. Tague C, Grant GE (2004) A geological framework for interpreting the low-flow regimes of cascade streams, Willamette river basin, Oregon. *Water Resour Res,* 40.
32. van Mantgem PJ, et al. (2009) Widespread increase of tree mortality rates in the western United States. *Science* 323:521–524.
33. Amos A (2014) Developing the law of the river: The integration of law and policy into hydrologic and socio-economic modeling efforts in the Willamette river basin. *U Kan L Rev* 62:1091.
34. McDonald RI, et al. (2011) Urban growth, climate change, and freshwater availability. *Proc Natl Acad Sci USA* 108:6312–6317.
35. Covich AP (2009) *Emerging Climate Change Impacts on Freshwater Resources. Resources for the Future Report* (Resour for the Future, Washington, DC).
36. Prudhomme C, et al. (2014) Hydrological droughts in the 21st century, hotspots and uncertainties from a global multimodel ensemble experiment. *Proc Natl Acad Sci USA* 111:3262–3267.
37. Elliott J, et al. (2014) Constraints and potentials of future irrigation water availability on agricultural production under climate change. *Proc Natl Acad Sci USA* 111: 3239–3244.
38. Harberger M (May 16, 2015) Farmer v. farmer: Future of Oregon water at center of fight over new dam in Silverton. The Oregonian, Business Section, p 1. Available at. www.oregonlive.com/business/index.ssf/2015/05/farmer_v_farmer_future_of_oreg.html.
39. Sen A (1981) *Poverty and Famines: An Essay on Entitlement and Deprivation* (Oxford Univ Press, New York).
40. Moore KM (2015) Optimizing reservoir operations to adapt to 21st century expectations of climate and social change in the Willamette River Basin, Oregon. Doctoral dissertation (Oregon State University, Corvallis, OR).
41. Howitt R, et al. (2015) *Economic Analysis of the 2015 Drought for California Agriculture* (UC Davis Center for Watershed Science, Davis, CA).
42. Goulden ML, Bales RC (2014) Mountain runoff vulnerability to increased evapotranspiration with vegetation expansion. *Proc Natl Acad Sci USA* 111:14071–14075.

Supporting Information (SI Appendix)

Jaeger et al. "Finding Water Scarcity Amid Abundance Using Human-Natural System Models"

1. System modeling overview

1.1. Model platform

The Willamette Water 2100 (WW2100) model was developed to generate spatial-temporal simulation pathways in the Willamette River Basin. It uses a platform called *Envision* developed at Oregon State University by John Bolte *(1)*. *Envision* consists of several hundred thousand lines of C++ code and runs as a 64-bit Windows application. The model of the landscape is made up of attributed map polygons called Integrated Decision Units (IDUs) that cover the spatial extent of the Willamette River Basin in Western Oregon, USA. The WW2100 Envision model incorporates a suite of sub-models to simulate processes that affect the distribution, movement, supply and demand for water in the Willamette Basin. As these component models run, they retrieve and store information from attributes within the IDU layer. The dataset archived here consists of 164,892 polygons attributed with starting values representing January 1, 2010, the first day simulated in model runs. Each IDU has 189 attributes representing landscape conditions including aspects of economics, land use, law, hydrology, climate, and vegetation (e.g., land use type, land value, annual maximum evapotranspiration (ET), and forest use predictive value). The program enables a range of different system components to interact and communicate via a representation of a landscape, a shared data repository that represents instantaneous conditions at specific locations. From a system perspective, each time the Envision model runs, it draws as its input, the outputs from other component models (e.g., hydrology, climate, farmer crop decisions, urban water use, reservoir management decisions) running within the framework. Envision synchronizes models as they step through time on their own time scales. For example, it runs a hydrological model with a daily time step 365 times before running, for example, an economic model with a yearly time step.

1.2. Spatial representation

Data are stored in ESRI shapefiles representing the stream network and landscape polygons called Integrated Decision Units (IDUs). The stream network and associated catchments were taken from the National Hydrography Dataset version 2 (NHD+V2) *(2)*. The IDU layer was developed by intersecting the catchment shapefile with a composite dataset representing land use and land cover in the Willamette Basin. This catchment shapefile provides information needed by the hydrology model to connect the landscape to individual stream reaches. The land use/land cover dataset was developed by combining information from two sources: i) a US Forest Service dataset (GNN) representation of the forested portions of the basin and ii) as US Department of Agriculture datasets (NASS CDL) representing all other portions of the basin.

The spatial configuration of these management-scale polygons (mean size = 19.2 ha) for forestland was based on Landsat remote sensing data and forest inventory data *(3, 4)*. The Integrated Landscape Assessment Project (ILAP) also provided a species-level vegetation classification. We assigned a stand age to each forested IDU based on overlay of the IDU coverage and a reference stand age coverage. For stand age ≤ 25, that coverage used Landsat-based LandTrender results *(5, 6)*, which evaluate the pixel-level trajectories of a vegetation-relevant spectral vegetation index. Stand age in 2010 was determined from the year of

disturbance. For stand age > 25, we used a stand age coverage derived from Landsat-based Gradient Nearest Neighbor Analysis *(7)*. Boundaries for land ownership and protection status were from the U.S. Geological Survey, National Gap Analysis Program *(8)*.

For nonforested land, the National Agricultural Statistics Service (NASS) data is derived from LANDSAT imagery and is designed to closely capture the crops grown as part of the agricultural system. There are 164,892 polygons in the IDU layer, covering the nearly 30,000 km^2 (11500 mi^2) extent of the Willamette River Basin. Most IDUs cover an area of between 2 and 700 hectares (5 and 1730 acres).

Daily time step processes include many processes such as stream flow, snowmelt, snow and canopy sublimation, infiltration and percolation, evapotranspiration, irrigation decisions, urban water use, and the exercise and enforcement of water rights. Annual time step processes include spatial distribution of population and income changes, expansion of urban growth boundaries, urban water price, crop choices, agricultural land value, forest wildfire, upland forest type, forest harvest, land use transition (for example from agricultural or forest uses to developed uses). Most WW2100 modeling scenarios simulate the period from January 1, 2010 through December 31, 2099. However, two scenarios were also run with a simulation period from January 1, 1950 - December 31, 2009 to allow comparisons of modeled future conditions to a modeled past. These scenarios used simulated historical climate data as a model forcing, but population, economics and land cover characteristics remained at 2010 levels.

Across the WW2100 study area, the initial land use on each IDU is determined by overlaying a set of spatial data layers, which include data from the US Geological Survey National Land Cover Data (NLCD)(http://landcover.usgs.gov/) and the USDA Cropland Data Layer (CDL)(https://nassgeodata.gmu.edu/).

1.3. Stream network

The stream network and associated catchments were taken from the National Hydrography Dataset version 2 (NHD+V2) *(2)*. Only the main flowpath, as defined by the NHD+V2 dataset, was used. The main flowpath does not diverge in the downstream direction, an assumption that is built into the routing model. It is a subset of the full NHD+V2 stream network derived from the stream network following directions provided by NHD+V2. The topological relationships between stream segments were defined using the ToNode and FromNode attributes of the NHD+V2 Value Added Attributes (VAA) table.

1.4. Feedbacks and linkages

Figure 1 in the article identifies some of the main linkages within and between the economic models and the biophysical models. Changes in the human system models over time are mainly driven by increases in population and income. These changes alter land prices and lead to development of agricultural and forest land. Population and income growth also result in changes in urban water use and water prices, and there are some changes in water use resulting from land use changes. Water use in agriculture is influenced by these land use changes as well as by the direct effects of climate on crop choice, crop water demand, irrigation decisions, and timing of farming practices, including planting.

Surface water diversions for irrigation and urban uses reduce streamflows, including those required for instream regulatory minimum environmental flows. As a result, low streamflows can trigger water shutoffs for relatively junior water right holders. These shutoffs

can affect farm income and farmland prices, which in turn influence the probability of land use change to alternative uses.

Water releases from federal reservoirs reflect detailed multiple-objective management rules that include protecting instream flows at various downstream control points. As a result, changes in downstream water use for cities and farms will feedback to influence reservoir releases, which in turn alter reservoir fill levels and benefits from reservoir recreation. Changes in forest land use including land development, tree planting and harvests, and wildfires will affect snow accumulation, sublimation, and melt; and forest evapotranspiration, all of which may have significant effects on streamflows.

2. Models of exogenous change

2.1. Selection and processing of climate scenarios

The World Climate Research Programme's Coupled Model Intercomparison Project (CMIP) is a worldwide effort to establish a set of standard experimental protocols for the use of general circulation models (GCMs), in the development of climate scenarios. Results from the CMIP project's latest phase, Phase 5, or CMIP5, began to be available around the time of the launch of WW2100. The WW2100 climate team saw an opportunity not just to use CMIP5 outputs but also to advance the evaluation and selection of GCMs. Since the elaborate set of models used in the WW2100 study could only accept a small number of climate scenarios, our goal was to use both quality and spread to select those scenarios.

2.1.1. Climate model evaluation

We assessed 41 GCMs from CMIP5 for their ability to simulate various aspects of climate *(9)*. The goal was "to evaluate model performance in order to make informed recommendations to those who may use these model outputs" *(9)*. We evaluated the models in their ability to replicate observed climate of the Pacific Northwest using a variety of metrics. These metrics included mean seasonal values, interannual variability, amplitude of the seasonal cycle, consistency in spatial patterns, and sensitivity to the El Niño Southern Oscillation, among others. To find the best fit, the team evaluated the CMIP5 GCMs according to their ability to recreate the observed climate of the 20th century and used two methods for combining the metrics; see *(9)* for details.

The result was a ranking of the models according to metrics that led to a subset of GCMs that the team's methods determined were the best statistical fit for the climate of the Pacific Northwest.

2.1.2. Selecting a small subset of climate scenarios

We selected a subset of three representative scenarios, from among the constellation of GCMs and future scenarios of greenhouse gases (representative concentration pathways, or RCPs), for use in the WW2100 constituent models. We used the approach developed for this project and described by *(10)*, in which a linearized impacts model is used to map the climate sensitivity space and select a small number of final scenarios that span that space while paying attention to the evaluation results described above. Specifically, we examined the response of June through September streamflow on the Willamette River (the season when scarcity is likely to emerge) to stepwise changes in temperature and precipitation, through the range of projected changes in temperature and precipitation from the subset of 33 CMIP5 climate models that were available at the time, with the RCP4.5 and RCP8.5 scenarios of future greenhouse gas

concentrations.

The sensitivity analysis uses simple perturbation experiments to estimate how much changes in temperature and precipitation affect summertime streamflow for the Willamette basin, using the Variable Infiltration Capacity (VIC) Macroscale Hydrologic Model. Then, a perturbation was introduced using the same set up, the hydrologic model was run again several times, but with incremental increases in temperature. The percent in which summertime streamflow changes in these perturbation experiments provides an estimate for how sensitive it will be in a warmer climate. The same type of perturbation experiments were then repeated but this time for both incremental precipitation increases and decreases.

From this calculation, we used the derived sensitivities to draw contours of constant summertime streamflow change on a scatter plot of temperature and precipitation changes as seen in GCM output. With the contours as guides, we selected GCMs and accompanying RCPs with the objective of spanning a wide range of hydrological impacts while preferring highly ranked models from the evaluation. We ended up selecting MIROC5-RCP8.5 as the reference case, because its projected change was near the all-model, all-RCP average. HadGEM2-ES-RCP8.5 represented the HighClim scenario, with one of the largest projected decreases in summer flow in the Willamette and a projected increase in annual mean temperature of 5.3°C for late 21st century.

The output of the climate models consists of daily data, and the coarse spatial resolution climate model results were then downscaled to the 4 km resolution of our other models using the Multivariate Adaptive Constructed Analogs (MACA) approach *(11)*. The key daily climate variables were solar radiation, precipitation, maximum temperature, minimum temperature, vapor pressure, and wind speed.

2.2. Population and income growth

Future population and income growth are assumed to be determined exogenously and, as such, they are external to the dynamics within the model, similar to the climate forcings. County-level population projections to 2050 and real (2005 dollars) mean household total personal income projections to 2040 are taken from the Oregon Office of Economic Analysis (http://www.oregon.gov/das/oea/Pages/Index.aspx) and Woods & Poole Economics, Inc. (http://www.woodsandpoole.com/), respectively. Linear extrapolation is used to obtain projections to 2100. Actual, forecasted, and extrapolated population and income by county and the period 1970-2100 are reported in Tables S1 and S2, respectively. For the 10 Willamette Basin counties, population increased at an average annual rate of 2.1% over the 1970-2100 period. The rate of increase is 1.2% over the period 2000-2050 and 0.8% over the period 2050-2100. For the 10 counties, mean household total person income increased at an annual rate of 1.9% over the period 1970-2010, and is projected to increase at a rate of 1.7% over the period 2010-2040 and 1.4% over the period 2040-2100.

3. Hydrology modeling

3.1. Overview

The Willamette Hydrology Model (WHM) was developed to capture potential effects of long term changes in climate, and also to incorporate the changes in the human system (land use change, water use) that interacted with the basin's hydrology. The model translates daily values of meteorological input (including precipitation, air temperature, wind speed, and radiation) into a spatially distributed estimate of water storage and release. It is run over the 90-year WW2100

scenario timeframe, and produces a dynamic estimate of the response of the hydrology to the evolving landscape and human system models. The model incorporates four overall elements describing key features of the basin's complex system:

(1) Mountain snowpack. Each winter, snow accumulates in the higher elevations of the Willamette valley. This natural reservoir serves to store a portion of the winter precipitation, releasing into streams (and reservoirs) during the spring. The model simulates the seasonal evolution of the mountain snowpack with a hybrid approach that includes the influence of both air temperature and radiation. The radiation-driven melt depends directly on vegetation, so that snow accumulation changes as forest disturbance and growth occurs over the scenario timeframe.

(2) Watershed hydrology. Incoming precipitation and snowmelt are stored within a set of conceptual reservoirs representing soil and groundwater. WHM defines the spatial distribution of those reservoirs based primarily on a set of approximately 9,000 sub-watersheds, defined by the National Hydrography Dataset *(2)*. Water is released from the subsurface conceptual reservoirs based on algorithms developed by Bergström and others *(12, 13)* as part of the HBV (Hydrologiska Byråns Vattenbalansavdelning) model. The released water then becomes stream discharge.

(3) Instream routing and reservoir storage. WHM uses a kinematic wave approach to simulate the flow of water within the stream network. The spatial pattern of the network was taken from NHD, and allows the model to estimate stream discharge throughout the watershed. Reservoir storage is a key feature of the Willamette River, and WHM incorporates the 13 largest reservoirs in the system – those managed by the US Army Corps of Engineers (USACE). Storage and release of water from the reservoirs is dictated by federal management rules and these are simulated using a version of the ResSim *(14)* model developed by USACE (see section S5.2).

(4) Water use. WHM integrates both biophysical and socioeconomic processes of water demand. The biological water demand for forests, crops and other vegetation is described in sections S3.3 and 3.6 below. The human use of water is determined in several economic models as the outcome of household and farm demand relationships and institutional constraints (e.g., profitability and law), as described in section S5. The economic models of human water demand interact in direct and indirect ways with the models of biological water demand, as in the case of crop water requirements and irrigation decisions.

3.2. Watershed hydrology model

The watershed hydrology model translates snowmelt and precipitation into soil moisture and stream runoff, using algorithms based on the well-established HBV model *(15)*. There are 3 primary rates that are defined by this component of the modeling: the partitioning of infiltrating water into a soil compartment and a fast runoff compartment, the recharge rate into a slow runoff compartment, and lastly, the rate of runoff of water into the stream network from the fast and slow runoff compartments.

Partitioning of infiltration: Water from precipitation as rain and snowmelt fills both the soil water and shallow runoff compartments. The proportion filling the soil compartment is defined as:

$$X = (soil/FC)^{\beta} \quad (1)$$

Where *soil* is the amount of water in the soil compartment (mm), FC a parameter representing the maximum amount of storage in soil compartment (mm), and Beta (β) a dimensionless

shaping parameter. Both FC and β are effective parameters found through calibration. The remaining proportion (1-*X*) recharges the fast response compartment.

Percolation: Percolation transfers water from the fast runoff compartment to the slow runoff compartment. It is defined as:

$$P=SUZ*PERC \quad (2)$$

Where *SUZ* is the amount of water in the fast response compartment (mm) and *PERC* is a calibrated parameter (day-1).

Runoff: Runoff is generated from the fast and slow response reservoirs. This runoff is defined as

$$Q = K_2*SLZ+K_1*SUZ+K_0*\max(SUZ-UZL,0) \quad (3)$$

Where K_0, K_1, and K_2 are calibrated recession coefficients (day-1), SLZ and SUZ represent the amount of water in the slow response compartment and fast response compartment, respectively, and UZL a threshold parameter.

3.3. Snow

Representation of snow accumulation and melt processes in WHM uses a modified version of the HBV degree-day model of Seibert *(16)*. Snow accumulation is governed by daily air temperature to determine the proportion of rainfall and snowfall from a precipitation event. Temperature is broken down into T_{min} and T_{max}, where T_{min} is the threshold below which all precipitation falls as snow, T_{max} is the threshold above which all precipitation falls as rain and at intermediate temperatures, precipitation is linearly partitioned into rain and snow. Based on calibration with observations and a validated model, T_{min} and T_{max} are prescribed to be -2 °C and 6 °C, respectively.

Snow accumulation is also governed by forest structure, as expressed by Leaf Area Index (*LAI*), which affects canopy interception and snow sublimation from the forest canopy.

Precipitation that is partitioned into snow is then reduced by a snowfall correction factor (*SFCF*), which accounts for the effects of snow sublimation from the forest canopy:

$$SFCF = fraction\ of\ max\_LAI * maximum\ SFCFI \quad (4)$$

where, *max_LAI* is set to 8 and the *fraction of max_LAI* is the LAI for the IDU divided by the *max_ LAI*. The *max_SFCF* is defined as 0.20 (20% of total snowfall during a single time step). This dimensionless factor adjusts for snow lost via evaporation and sublimation from the forest canopy and the snowpack, which is not simulated explicitly *(17)*. The amount of snow sublimated, *snow_evap*, is the total snowfall multiplied by SFCF:

$$snow\_evap\_mm = snow\_total\_mm * SFCF \quad (5)$$

and the snowfall that becomes part of the snowpack is:

$$snow\_thrufall\_mm = snow\_total\_mm - snow\_evap\_mm \quad (6)$$

The degree-day factor, also termed melt factor, is represented in WHM by a variable called *CFMAX*. The degree-day factor represents the rate at which a unit mass of snow is melted by convective energy for a given energy input (mm $^{o}C^{-1}$ d^{-1}); it uses air temperature (T_a) as a proxy for total energy input to the snowpack. Snowmelt (mm d^{-1}) is computed as:

$$convective\_melt\_mm = CFMAX * (T_a - TT) \quad (7)$$

where, *TT* is the threshold temperature above which snowmelt is considered to occur. *TT* is set to 0°C. The value of *CFMAX* is determined through calibration. Calibrated values of *CFMAX* are, however, constrained to the range $2.5 < CFMAX < 6.0$ determined through offline testing. Two other variables, the water holding capacity (*CWH*) and the refreezing coefficient (CFR) are both

considered insensitive parameters in snow modeling *(16)*. *CWH* was held constant at 0.1. *CFR* was included in the set of calibrated parameters, but constrained to values in the range [0, 0.1].

We use the same approach as in the Biome-BGC ecosystem process model *(18)* to compute the snowmelt due to radiant energy transmitted through the forest canopy. Shortwave transmittance (*sw_trans*, kJ/m^2/d) through the canopy is computed as a function of LAI (using Beer's Law) and then radiative melt is computed when air temperature exceeds *TT*, as below:

$$radiative\_melt\_mm = swtrans / lh\_fus \quad [mmH_2O/d] \qquad (8)$$

where, *lh_fus* is the latent heat of fusion (335.0 kJ/kg).

Snowmelt is constrained by the amount of actual snow available in each IDU and when snowmelt exceeds the water holding capacity of the snowpack, melt is routed into the soil.

3.4. Upland forest evapotranspiration

As noted, we used a polygon-based landscape simulation model, *Envision (1*) to annually update the land cover and leaf area index, as impacted by forest growth (aging) as well as land use change and disturbances (forest harvest and wildfire). As with the agricultural lands hydrology modeling (described below), an existing watershed hydrology model (HBV)*(15)* was adapted for use in the upland forest hydrology modeling *(19)*. The WRB version (Willamette Hydrology Model, WHM) generates daily-time-step estimates for evapotranspiration (transpiration + soil evaporation).

An initial LAI-specific potential daily ET rate was determined based on the Penman-Monteith approach *(20)*, with inputs of solar radiation (for estimation of net short wave radiation), air temperature (for estimation of saturation vapor pressure and net long wave radiation), vapor pressure (for estimation of vapor pressure deficit), and LAI (for estimation of bulk stomatal resistance), as well as wind speed and stand height (for estimation of canopy aerodynamic resistance). Surface albedo was assumed to be 0.15 *(21)*. Reference stomatal resistance was based on Kelliher et al. *(22)*. The potential ET was then modified by scalars (0-1) based on soil water status and vapor pressure deficit (VPD) to determine the actual ET_{PM}, with only the lower of the 2 scalars applied on any given day. The soil water scalar is a linear ramp from 1 to 0 based on the ratio of current SW to available soil water (field capacity - wilting point capacity). The ramp begins at 1.0 for a ratio of 0.5 and decreased to 0 for a ratio of 0. The VPD scalar is described as:

$$VPD_{scalar} = (1 - ((VPD - VPD_{min})/(VPD_{max} - VPD_{min}))) \qquad (9)$$

where VPD_{min} (0.610MPa) and VPD_{max} (3.100MPa) are based on observations in coniferous forests at the leaf level *(23)* and at eddy covariance towers *(24)*. VPD_{scalar} was set to 1.0 below VPD_{min} and set to a minimum of 0.02 as VPD approaches VPD_{max}. The VPD scalar accounts for the observations that conifer transpiration in the Pacific Northwest is generally sensitive to VPD *(24, 25)*. Under low LAI conditions, aerodynamic resistance would be high, so the VPD scalar has little effect. In the Pacific Northwest summer (generally warm and dry), the litter/upper soil would be dry under high VPD conditions and soil surface resistance would be high in any case.

3.5. Agricultural evapotranspiration

Evapotranspiration (ET) is simulated daily for each IDU and is then spatially aggregated to the HRU (Hydrologic Response Unit) level (described in S3.4.1). The rate of daily ET is modeled as a dynamic function of the climate, land cover, soil water, and crop phenology. The reference evapotranspiration is determined using the FAO-56 method *(26)*, and further developed

for Idaho *(27)*. The potential (maximum) evapotranspiration (*MAX_ET*) or water demand of the crop is then calculated based upon the reference evapotranspiration. In the model, potential evapotranspiration represents the rate of maximum evapotranspiration of a healthy crop under no water stress. The idea is the crop is growing in large fields under optimum agronomic and irrigation management conditions, so if it were irrigated, evapotranspiration would not exceed potential evapotranspiration. This *MAX_ET* value is then reduced to an actual ET (AET) based on the available water in the soil water reservoir.

The reference evapotranspiration – crop cover approach consists of two steps. First, the evapotranspiration for a theoretical, uniform, well-watered crop is calculated; this is considered the reference evapotranspiration (ET_r). This reference ET_r value is then multiplied by a land cover coefficient (K_c) to approximate the maximum evapotranspiration (*MAX_ET*) for the specific land cover at that location. The governing equation for this maximum is thus:

$$MAX\_ET_{land\ cover} = ET_r * K_c \quad (10)$$

In the model, ET_r is estimated using the FAO-56 method, which is based on a 2005 ASCE Standardized Reference Evapotranspiration equation, known as Penman-Monteith FAO-56 method equation *(20)*, using the tall alfalfa reference crop:

$$ET_r = \frac{0.408\Delta\,(R_n - G) + \frac{\gamma C_n}{T+273} u_2 (e_s^o - e_a)}{\Delta + \gamma(1 + C_d u_2)} \quad (11)$$

where T is the mean air temperature (^{0}C), u_2 is the wind speed (m s^{-1}) at 2m above the ground, R_n is the net solar radiation (MJ m^{-2} d^{-1}), Δ is the slope of the saturation vapor pressure and mean air temperature curve, γ is the psychrometric constant (kPa ^{0}C^{-1}), the term $(e_s^o - e_a)$ is the daily vapor pressure deficit, G is the daily soil heat flux density, taken to be 0 in this model, C_n = 1600 and C_d = 0.38 are constants for a tall Alfalfa reference.

The ET_r calculation requires daily input values of air temperature, solar radiation, humidity, and wind speed. These climate data were supplied using 4-km downscaled meteorological data from the University of Idaho *(11)*.

The land cover coefficient, K_c, represents the ratio of the *MAX_ET* of a specific land cover to the evapotranspiration calculated for a tall reference grass (Alfalfa*)(27)*. Land cover coefficient curves have been developed for many agricultural crops in the Pacific Northwest by the US Bureau of Reclamation (http://www.usbr.gov/pn/agrimet/index.html) and others as documented in *(27)*. The curves represent the crop coefficient at various times throughout the growing season. Based on the current stage of growth of the crop, the appropriate coefficient can be interpolated from the curve and multiplied by the ET_r to find the daily *MAX_ET*. By this method, the value of K_c is dependent on the phenology of the crop.

The growth stage of each crop was determined using a modified approach to that described by Allen and Robison *(27)* and then crop curves were dynamically applied on an annual basis. Allen and Robison define four methods of applying crop curves; however, the scope of our project required a somewhat simplified approach. We estimated a planting or green-up date to start the application of the crop curve, a harvest or dormancy date to end the application of the curve, and defined an interpolation method for applying the curve between these dates. These methods varied by land cover. Outside of the growing season, we applied a constant coefficient equal to the first value of the crop curve for that land cover.

One of two methods was used to estimate the planting or greenup date:

i. The average of the daily temperature for the thirty days prior to the current day. Once this value reaches a crop-specific threshold, signal planting.
ii. Cumulative growing degree days from January 1 to the current day are calculated. Once this value reaches a crop-specific threshold, signal planting. Cumulative growing degree days are a measure of accumulated heat units available to the plant for growth and are calculated using one of the following equations:

$$GDD = \max(T_{mean} - T_{base}, 0) \quad (12)$$

$$GDD_{corn} = \frac{\max(min(T_{max},30),10)+\max(\min(T_{min},30),10)}{2} - 10 \quad (13)$$

where T_{max}, T_{min}, and T_{mean} refer to the maximum, minimum, and mean daily air temperature ($°C$), respectively. T_{base} is a threshold temperature for each crop at which growth is assumed to occur. Note that all crops except corn used the first equation.

To determine the harvest date, or dormancy date for perennials, we used one of three methods:

i. The accumulated growing degree days from planting date is calculated. Once this value reaches a crop-specific threshold, signal harvest.
ii. The occurrence of a killing frost signals harvest.
iii. The earlier of conditions described above in i. or ii. signals harvest.

The planting and harvest dates mark the temporal endpoints for which the crop curve is applied. One of two interpolation methods was then used to apply the individual crop coefficients:

i. Accumulated growing degree days between planting and termination dates.
ii. Accumulated growing days between planting and termination dates.

For both interpolation methods, land cover-specific threshold values are defined that allow the model to identify what percentage of growth the land cover is in relative to the total growing season.

The process described above produces a maximum (potential) evapotranspiration value for each IDU for each day. This is assumed to be the *MAX_ET* from that IDU if there were no soil limitations. Given that the soil water reservoir is not infinite, an additional step was used to convert the *MAX_ET* to an AET. Seibert *(28)* outlines this function as part of the soil moisture routine used in the HBV-Light model. The ratio of AET to *MAX_ET* is a function of the soil moisture as illustrated in Fig S1 modified from Seibert *(28)*,

$$where\ \Theta_t = 0.5\ (\Theta_{FC} - \Theta_{WP}) \quad (14)$$

The parameters Θ_{FC} and Θ_t represent the maximum soil moisture storage and the amount of soil moisture storage above which the AET equals the *MAX_ET*, respectively. The parameter Θ_{WP} represents the minimum value of soil moisture for ET to occur. If the soil moisture amount is less than Θ_{WP}, no ET occurs. If the soil moisture amount is greater than Θ_t, AET is equal to *MAX_ET*. At soil moisture values between Θ_{WP} and the threshold, $\Theta_t = 0.5(\Theta_{FC} - \Theta_{WP})$, AET is reduced linearly. Θ_{FC} is a calibrated parameter found during calibration; Θ_{WP} is a constant 10 mm, and Θ_t is a constant 0.5. The equations governing the rate of ET given the amount of soil moisture are as follows:

$$ET_{soil\ moisture<\Theta_{WP}} = 0 \quad (15)$$

$$ET_{\Theta_{WP}<soil\ moisture<\theta_t} = MAX\_ET * \frac{1}{\Theta_t - \Theta_{WP}} * (soil\ moisture - \Theta_{WP}) \quad (16)$$

$$ET_{soil\ moisture>\Theta_t} = MAX\_ET \quad (17)$$

The AET calculation represents the amount of water the crop used. Once the AET is calculated, this value is removed from the soil moisture reservoir, reducing the amount of water available in the HRU. In our case, two soil moisture reservoirs were created in each HRU, one for irrigated and one for non-irrigated IDUs.

3.6. Water routing

The method for routing instream flows is a kinematic approach that follows directly from a solution developed by Chow et al. *(29)*. The method is a simplification of the St. Venant equations describing free surface flows. The full St. Venant approach represents the conservation of mass and momentum and can be represented by two relationships, one for continuity:

$$\frac{\partial Q}{\partial x} + \frac{\partial A}{\partial t} = q \quad (18)$$

and one for conservation of momentum:

$$\frac{1}{A}\frac{\partial Q}{\partial t} + \frac{1}{A}\frac{\partial}{\partial x}\left(\frac{Q^2}{A}\right) + g\frac{\partial y}{\partial x} - g\left(S_0 - S_f\right) = 0 \quad (19)$$

Local acceleration Acceleration | Convective acceleration Acceleration | Pressure Force | Gravity Force | Friction Force

These two equations fully describe discharge as a function of both time and space, and a direct solution to these equations is typically referred to as a dynamic solution. Simplifications are commonly employed however, and rely upon a variety of assumptions about the movement of water and the importance of different terms. The kinematic wave is one such simplification. If the kinematic wave dominates the hydrograph, the acceleration and pressure force are negligible and the model simplifies to the statement that gravity forces equal friction forces. In other words, within each element of time and space the discharge does not change, a situation commonly referred to as uniform flow. In the event that the flow can be considered uniform, the momentum equation can be replaced with a standard uniform resistance equation such as Manning's or the Chezy equation. A commonly cited version of the kinematic flow equation, using Manning's equation, is:

$$\frac{\partial Q}{\partial x} + \alpha\beta Q^{*\beta-1}\left(\frac{\partial Q}{\partial t}\right) = q \quad (20)$$

In this equation, alpha and beta are parameter combinations from Manning's equation.
A finite difference solution for the kinematic wave equation can be developed by assuming

$$\frac{\partial Q}{\partial x} = \frac{Q_{time} - Q_{time-1}^{in}}{\Delta x} \quad (21)$$

$$\frac{\partial Q}{\partial t} = \frac{Q_{time} - Q_{time-1}}{\Delta t} \quad (22)$$

$$Q^{*} = \frac{Q_{time-1} + Q^{in}}{2} \quad (23)$$

which when substituted into equation (20) above can solved for the unknown value Q_{time}. Assuming that $z = \alpha\beta Q^{*\beta-1}$ the finite difference solution becomes

$$Q_{time} = \frac{q_{time} + \frac{Q^{in}}{\Delta x} + z\frac{Q_{time-1}}{\Delta t}}{\left[\frac{1}{\Delta x} + \frac{z}{\Delta t}\right]} \quad (24)$$

This equation represents the unknown value of Q as a function of known values related to upstream discharges, previous time discharge, and normal flow parameters and was developed by Chow et al. *(29)*.

3.7. Hydrology model calibration

3.7.1 Overview

The watershed hydrology model (WHM) uses the HBV runoff model *(12, 16)*. It was calibrated using streamflow records from the US Geological Survey and, for snowy headwater sub-basins, snow water equivalent records from the Natural Resources Conservation Service (http://www.wcc.nrcs.usda.gov/snotel/SNOTEL_brochure.pdf). The rainfall-runoff model within WHM has nine calibration parameters related to snowfall, runoff, and percolation. Calibration of these parameters affects the flux between the conceptual reservoirs shown in Figure S2.

The calibration was undertaken in three stages. First the headwater reservoir drainages were calibrated, then the tributary basins, followed by selecting parameter values for the remaining areas where it was not possible to calibrate directly based on observed flow data. We note that some portions of the basin did not have adequate data on discharge or estimates of natural flows due to poor data or for which significant human interventions in natural flows that could not be corrected. Calibration was performed using the PEST parameter estimation program (www.pesthomepage.org). Sets of nine HBV parameters were estimated for nine reservoir drainages in the WRB: Cottage Grove reservoir, Dorena reservoir, Fern Ridge reservoir, Blue River reservoir, Cougar reservoir, Fall Creek reservoir, Hills Creek reservoir, Detroit reservoir, and Green Peter reservoir.

The WW2100 HBV model includes the following compartments for water in each HRU: snowpack, snow water, unirrigated topsoil, irrigated topsoil, subsoil, groundwater. Snowpack and snow water are the frozen and unfrozen water in the snowpack. Irrigated and unirrigated topsoil represent the same soil layer for IDUs that are irrigated versus unirrigated in each HRU (an HRU may include IDUs that are irrigated and others that are unirrigated, depending on water rights and farmer decisions in the economic models).

The calibration period was 1980-1994, for which measured data sets used in the calibration process included USGS stream gage records, NRNI synthetic flow data, Oregon NRCS Snowpack Telemetry (SNOTEL) snow water equivalent data, and measured inflow data

for federal reservoirs. The model was run for the calibration period using meteorological forcings from MACA *(Multivariate Adaptive Constructed Analogs)* training data derived from observed weather station data. The nine parameters produced good correlations between modeled estimates and observed datasets. Comparisons of observations and simulations after calibration showed generally good correspondence (e.g. streamflow, Table S3).

3.7.2 Calibration details

The WW2100 HBV model calculates daily HRU fluxes from surface (rain and snowmelt) to topsoil (infiltration), surface to subsoil (subsoil recharge), subsoil to groundwater (percolation), subsoil to stream (q0), and groundwater to stream (q2).

The nine estimated parameters in the calibration are the following:

1. CFMAX: the amount of snow that will melt per day per deg C above 0 °C; measured as mm of SWE.
2. CFR: the refreezing coefficient; when the snow temperature is below the 0 °C snow temperature threshold, some water in the snowpack will refreeze. The amount of water that refreezes, in mm, is CFR*CFMAX per day per deg C below the snow temperature threshold.
3. FC: field capacity of the topsoil; used in calculating the subsoil recharge fraction, which is the fraction of the incoming rain and snowmelt that bypasses the topsoil and goes directly to the subsoil. The subsoil recharge fraction is calculated as the amount of water currently in the topsoil (to be exact, the amount above 10 mm, taken as the wilting point), expressed as a fraction of FC, raised to the power BETA. When the topsoil is already at field capacity, all the incoming water bypasses the topsoil and recharges the subsoil.
4. BETA: for subsoil recharge; used to calculate the subsoil recharge fraction. See the description under FC above.
5. PERC: fraction of water in subsoil pool that percolates down to groundwater pool each day.
6. UZL: the soil water threshold value in mm which is used in the decision about which of two forms of the q_0 calculation to use. q_0 is the amount of water that flows from the subsoil to the stream each day. When the water content of the subsoil is above UZL, q_0 is calculated as:

K0*(subsoil water content - UZL) + K1*subsoil water content

When the water in the subsoil is at or below UZL, q_0 is:

K1*subsoil water content

7. K0: a dimensionless constant used in the calculation of q_0, the water that flows from the subsoil to the stream. See the description under UZL.
8. K1: a dimensionless constant used in the calculation of q_0, the water that flows from the subsoil to the stream. See the description under UZL.
9. K2: a dimensionless constant, the fraction of the groundwater pool that flows to the stream each day.

For each daily run of HBV, an evapotranspiration function calculates evapotranspiration from each IDU based on HBV soil moisture and other inputs.

The spatial and temporal flows in the hydrology model are captured in an autonomous process within the *Willamette Envision* framework that simulates daily and annual flows of water in the stream network, taking account of runoff from HBV, irrigation withdrawals, municipal withdrawals, returns from municipal treatment plants, and reservoir operations (as described in more detail elsewhere). The Willamette Hydrology Model (WHM) integrates natural system hydrology along with both private behavior in the human system (cities and farms) and public management (reservoir operations)

In the first stage of the calibration, reservoir inflow records were used to represent observed gage data. The PEST parameter estimation program was used with a "Flow-only" version of the WW2100 model (human system and other components turned off), using MACA daily weather training data to obtain sets of parameter values applicable to the areas which drain into the 9 reservoirs indicated above. Dexter reservoir and Big Cliff reservoir were omitted because they are reregulating reservoirs. Lookout Point reservoir was omitted because it is in the same drainage as Hills Creek reservoir. Foster reservoir was omitted because it is downstream of Green Peter.

For drainage areas below the reservoirs for which no-reservoir-no-irrigation (NRNI) synthetic gauge data is available, PEST was used with a Flow-only, no-reservoir version of WW2100 on MACA daily weather training data to obtain an individual set of parameter values applicable to each such area. This stage was possible for an additional five sub-areas.

The parameter values resulting from the calibration procedures are included, along with constraints on parameters, in the Table S4 below. In addition to constraints imposed by the HBV model, additional constraints were introduced to limit the range of parameter values based on those reported in other HBV studies *(30-33)*.

4. Landscape modeling

Landscape characteristics are determined in part by human land use decisions. This includes public or policy choices (public lands, urban growth boundaries, regulations), and private decisions in land markets. Population and income are key drivers of land markets and the prices or values for developed land uses. As population and household incomes increase, demand for developed urban land typically increases as well, leading to an increase in land value and a transition from agricultural and forest uses into urban uses. Understanding future population and income growth is paramount to anticipating shifts in land use and the resulting impacts on water. Within the model, relative values of land in different uses determine changes in land use over time. Urban growth boundaries (UGBs), an integral part of Oregon's land-use planning system, constrain where development can occur and are adjusted periodically as a city's population grows.

4.1.1 Land use, land values and land-use change

Across the WW2100 study area, the initial land use/land cover on each IDU is determined by overlaying a set of spatial data layers, which include data from the National Land Cover Database (NLCD) and Cropland Data Layer (CDL), as described in S1.2. The land-use change component of the WW2100 model simulates decisions to change land between agricultural, forest, and urban uses as a function of the economic returns to those uses. The economic returns are estimated on the basis of site characteristics such as farm rents (annual net returns to farming), distances to cities, and population and income of nearby cities. Returns to land and land-use transitions also are influenced by urban growth boundaries (UGBs). The land-use component includes a mechanism by which UGBs expand over time (described below).

Changes between forest, agriculture, and urban land uses are the focus of the WW2100 land-use change model, since these are the major uses, and sources of land-use change, that occur within the Willamette River Basin study area *(34)*. In addition, the property value data used to parameterize the economic returns to different land uses are not readily available for more disaggregated land use categories (e.g., specific crops or forest types). Differences within

each of these broad land-use categories are controlled for by including separate sets of explanatory land characteristics in each land value equation.

The scope of the land-use transitions model is limited to privately-owned lands, as the bulk of land-use change in our study area is due to decisions made by private actors. Wetland areas are not allowed to change uses, in accordance with local and federal planning rules and regulations that discourage wetland conversion. In addition, it is difficult to determine the market value of wetlands, since they do not easily fit into any one of the three categories we consider, and much of their value stems from recreation and nonmarket ecosystem service provision (e.g., water filtration). Bidirectional transitions are allowed between privately-owned forest and agricultural land anywhere in the study area. Land development, on the other hand, or the conversion of forest or agricultural land to an urban use, is restricted to occur within urban growth boundaries (UGBs), which, as mentioned above, are allowed to expand over the course of the model simulations. Development is also considered to be irreversible for the purposes of the WW2100 model (i.e., transitions from urban to agriculture or forest are not allowed).

4.1.2 Estimating economic returns to different land uses

Parcel-level data on real (inflated adjusted) market values of developed, agricultural, and forest lands were collected for four counties (Benton, Lane, Marion, and Washington) in the Willamette Basin. The four sample counties were selected to represent the major urban areas within the Willamette River Basin (Corvallis, Eugene-Springfield, Salem, and Portland Metro), and to cover the geographic extent of the WRB (see Bigelow *(35)* for more details). The parcels included from each county were stratified according to three broad land use categories: agriculture, forest, and residential development. Random samples for each land use were then drawn, with final sample sizes as follows: Benton (430), Lane (1,134), Marion (1,576) and Washington (1,599). The relative size of the county samples are proportional to the sizes of the urban areas they represent. Observations were obtained for the years 1973, 1980, 1986, 1992, and 2000, making it possible to use panel data methods to estimate a hedonic land value model for each of the three major land uses considered. The set of variables, definitions, and data sources are described in Table S5.

Equation 25 illustrates the general form of the hedonic models that were estimated:

$$ln\left(V_{it}^{j}\right) = \beta_{0it}^{j} + \sum_{k=1}^{K_j} \beta_{kit}^{j} X_{kit}^{j} + \mu_{i}^{j} + \varepsilon_{it}^{j}, \quad (25)$$

where the dependent variable, $ln\left(V_{it}^{j}\right)$, denotes the natural log of the per-acre, inflation-adjusted land value for parcel i in use j at time t. Additional terms in equation 25 denote the use-specific constant term (β_{0it}^{j}), use-specific covariates (X_{kit}^{j}) and their associated parameters (β_{kit}^{j}), where the number of covariates (K_j) varies by land use, a parcel-specific error component (μ_{i}^{j}), and a standard idiosyncratic error term (ε_{it}^{j}).

The model estimation results are summarized in Table S6. The developed land value equation was estimated using a Hausman-Taylor *(36)* model, which allows for certain covariates in the model to be treated as endogenous and does not require the use of external instruments (e.g., *37*). In our case, the time-invariant effect of a parcel being located within an urban growth boundary (UGB) was treated as endogenous. The area covered by a given municipality's UGB is determined by city planners who, when setting the UGB boundaries, were likely to target land parcels with characteristics that make them suitable for urban land uses. If there are unobserved

factors that influenced both the decision to place a parcel within a UGB and the subsequent value of that land, the UGB effect will not be properly identified.

In modeling the land values for forest and agricultural uses, a more general method was used to control for unobserved parcel heterogeneity that could influence land values. Specifically, the results were derived using a correlated random effects (CRE)*(38)* estimator. This approach entails including the parcel means of the time-varying explanatory factors in the model as additional regressors, and provides a way to generate parameter estimates for time-invariant land characteristics, such as soil quality and topography, which are important determinants of the value of land in undeveloped use.

4.1.3. Predicting economic returns to different uses

Initial estimates of agricultural and forest land values included several factors that convey a parcel's potential for development (e.g., population density, household income). For the purposes of predicting land use transitions as a function of the relative economic returns to developed, agricultural, and forest uses, the values of land being converted to or kept in a forest or agricultural use should not be confounded by the capitalization of expected future development rents. To accomplish this, prior to using the forest and agricultural land value estimates the coefficients on population density and household income in (25) were set to zero. The UGB distance variable was also set to zero for predictions in the agricultural land value equation for similar reasons.

Additional adjustments were made prior to using the hedonic model estimates for prediction in the WW2100 simulations. First, the Year and UGB*Year terms were all assumed to take on the coefficients pertaining to the year 2000. Each model in Table S6 contains an inverse Mill's ratio (IMR; and its mean, in the forest and agriculture equations) variable. This variable is derived from a set of panel sample selection models, estimated with the approach given in Wooldridge *(39)*, to account for the unbalanced structure of the land value panel datasets (see (*35)* for more detail). For the purposes of using the models for prediction in the WW2100 simulations, each of the use-specific IMR variables is set to one. Additionally, there is a large discrepancy between the size of the developed land parcels used in the developed land hedonic equation and the WW2100 simulation model IDUs. In order to assure that development decisions are made at the average lot size observed in the underlying hedonic model data, the average observed developed parcel size (0.39 acres) was used to compute developed land returns. Not doing so would substantially reduce the developed land values that drive urbanization. Last, the estimated hedonic models also contain variables representing the value of improvements on each parcel. Since land improvements (e.g., houses and barns) are not accounted for in the WW2100 simulations, the average improvement value for each land use is set to its average value observed in the underlying hedonic model input data.

The dependent variable in each land value equation is the logged per-acre value of land. To obtain the unlogged predictions, the exponent of each predicted value is computed and multiplied by a correction factor listed at the bottom of Table S6. For example, the developed land value prediction is given by $e^{ln(V_{it}^{D})} * 1.035$. This adjustment is required to remove any bias stemming from the standard assumption in linear regression models that the disturbances are normally distributed, which does not necessarily apply in our case due to the log-transformation of the hedonic dependent variables *(40)*.

The estimated hedonic model for each land use contains a set of county dummy variables to control for unobserved county-level heterogeneity. In using these models for prediction in the

WW2100 simulation, the county dummy coefficients are applied to the four counties that comprised the samples used to estimate the hedonic models, and to the other counties in the basin based on their proximity to the four original study counties. Predictions with the county dummy variables in non-sample counties are made as follows: the Washington County coefficient is applied to IDUs in Clackamas, Columbia, Multnomah, and Yamhill counties; the Lane County coefficient is applied to IDUs in Douglas county; Marion County was the omitted, baseline county, and is assumed to represent IDUs in Linn and Polk counties.

4.1.4 Land-use change model

In the WW2100 model, each IDU is described by a set of attributes, including land cover. Starting from an initial land cover map for 2011, we model changes in land use as a function of the land values described in Section S4.1.2. With three uses (agriculture, forest, developed), there are a total of nine possible transitions (counting transitions in which land does not change use; e.g., forest-to-forest). This number is reduced to six because land that is in developed use is assumed to remain in that use indefinitely. Thus, we are concerned with the six transitions in Table S7. In particular, we model the probability that each transition takes place, where P_{jk} indicates the probability that land moves from use j to use k (e.g., P_{af} is the probability that land moves from j=agriculture to k=forest). Because land must end in one of the three categories, it follows that $P_{aa} + P_{af} + P_{ad} = 1$ and $P_{ff} + P_{fa} + P_{fd} = 1$.

For those IDUs that begin 2011 in agriculture or forest and are categorized as privately-owned, we define the six probabilities indicated above as logistic functions of economic returns to agriculture, forest, and development. Formulas given below are used to compute transition probabilities for each 5-year time period for each IDU. Calculation of these transition probabilities requires three steps. First, we use the equations described in S4.1.2, together with data on with IDU characteristics, to calculate dev_val, ag_val, and for_val for each IDU. Note that some of the IDU attributes are fixed over time (e.g., slope) but others, such as population and income of the nearest city, change according to the procedure described in Section 2.2.

Second, the computed economic returns (dev_val, ag_val, and for_val) are scaled using formulae given in Table S8. The scaling is necessary because the parameters in the transition probability formulae were obtained from Lewis et al. *(41)*, in which a model of land-use transitions for western Oregon and Washington was estimated using land-use data from the National Resources Inventory and measures of economic returns from *(42)*. Thus, if an IDU begins in forest, the economic return to agriculture on that IDU is found by first computing ag_val , multiplying ag_val by 0.01, and then (if necessary) constraining the result to lie between 0 and 2000. The scaled/constrained values of the economic returns are denoted AR_a, FR_a, and DR_a when the starting use is agriculture and AR_f, FR_f, and DR_f when the starting use is forest. Because $DR_f = DR_a$, we will simply refer to this value as DR.

Once the values of AR_a, FR_a, and DR or AR_f, FR_f, and DR are determined for each IDU, the third step is to plug them into formulas that determine the five-year transition probabilities, as given in *(42)*. Specifically, for IDUs starting in agriculture, the five-year transition probabilities are given by:

$$P_{aa} = \frac{e^{0.00489AR_a}}{e^{0.00489AR_a} + e^{-7.799+0.00242FR_a} + e^{-4.788+0.00013DR}} \quad (26)$$

$$P_{af} = \frac{e^{-7.799+0.00242FR_a}}{e^{0.00489AR_a}+e^{-7.799+0.00242FR_a}+e^{-4.788+0.00013DR}} \quad (27)$$

$$P_{ad} = 1 - P_{aa} - P_{af} \quad (28)$$

For parcels starting in forest, the five-year transition probabilities are given by:

$$P_{ff} = \frac{e^{0.00489FR_f}}{e^{0.00489FR_f}+e^{-7.799+0.00242AR_f}+e^{-4.788+0.00013DR}} \quad (29)$$

$$P_{fa} = \frac{e^{-7.799+0.00242AR_f}}{e^{0.00489FR_f}+e^{-7.799+0.00242AR_f}+e^{-4.788+0.00013DR}} \quad (30)$$

$$P_{fd} = 1 - P_{ff} - P_{fa} \quad (31)$$

With the WW2100 model, we wish to represent land-use change on an annual basis. To this end, the five-year probabilities are converted to equivalent annual probabilities. Specifically, if P_{jk} is the five-year transition probability, then the corresponding annual transition probability (AP_{jk}) is given by:

$$AP_{jk}=1-(1-P_{jk})^{0.2} \quad (32)$$

When the model is run, the annual probabilities are used for a five-year period and then updated. Given sets of values of AP_{jk} for each IDU, the final step is to determine whether or not land-use changes actually occur on an IDU. For this, we use a random number generator. Suppose that a given IDU is currently in agriculture and has a 0.8 probability of remaining in agriculture (i.e., AP_{aa}=0.80), a 0.1probability of switching to forest (AP_{af}=0.10) and a 0.1probability of switching to developed use (AP_{ad}=0.10). We draw a random variable r from a uniform distribution defined on the unit interval. The IDU remains in agriculture if $0.8>r\geq 0$, changes to forest if $0.9>r\geq 0.8$, and changes to developed use if $1.0\geq r\geq 0.9$. This procedure is repeated for each IDU using newly-drawn values of r. At the end of this process, a new land-use map is produced.

Zoning and UGB expansions

To account for zoning rules under Oregon's land-use planning system, we treat land inside and outside of UGBs differently. Land outside of UGBs can move between undeveloped uses (i.e., ag-to-forest and forest-to-ag transitions are allowed) but transitions to developed use are not allowed. To account for this restriction on development, the transition probabilities need to be adjusted. For IDUs outside of UGBs, the probability associated with the transition to developed use is added to the probability associated with the land remaining in the same use. Thus, if the initial use is agriculture, $P_{aa}(new) = P_{aa}(old) + P_{ad}$. If the initial use is forest, $P_{ff}(new) = P_{ff}(old) + P_{fd}$. These restrictions on development are also applied to areas zoned as rural residential (which are outside of UGBs) since only a small portion of the lot is allowed to be developed.

For IDUs inside of UGBs, all of the transitions are allowed. Given the irreversibility of development, it follows that, over time, the share of developed land within each UGB will increase. To mimic the land-use planning process, we allow for UGBs to expand once the developed share becomes sufficiently large. The developed share is defined as the ratio of the area of private land within a UGB that is developed to the area of private land within a UGB that is developable. Developable land includes all private land that is in developed, agriculture, other

vegetation, and forest categories. It excludes land in the barren, wetlands, and water/snow/ice categories. As long as the developed percentage of the UGB is below a specified threshold, the existing UGB remains as it is. The threshold is 80% in the reference case, except for Eugene-Springfield where 70% was used in recognition of the on-going UGB expansion process during our model's development (2010-2015). However, once the threshold is exceeded, a UGB expansion is triggered. We assume that the need for a UGB expansion is evaluated every five years, coinciding with the updating of the five-year transition probabilities.

A UGB expansion involves adding new IDUs to the existing UGB area until the specified threshold is no longer exceeded. Which IDUs to add is determined by the following criteria:

1) Only select IDUs that are adjacent to the existing (or expanded) UGB area.
2) Only select IDUs that are privately-owned and developable (i.e., in developed, agriculture, other vegetation, or forest categories).
3) Do not select IDUs that are already inside another UGB.
4) Select IDUs in order of least equally-weighted distance from: (a) the centroid of the IDU to the center of the UGB area, and (b) the centroid of the IDU to the nearest major road.
5) Do not select IDUs that are zoned for exclusive farm use (EFU) or forest conservation (FC) unless there are no other IDUs that satisfy criteria 1-3 and the developed percentage is still higher than the prescribed threshold. Once the non-EFU and non-FC IDUs that satisfy criteria 1-3 are exhausted, continue selecting IDUs that are zoned as EFU or FC using criteria 4 until the developed land percentage is again below the prescribed threshold.

These criteria do not apply to expansions in the Portland Metro UGB. In this case, the regional planning authority (Metro) has designated areas called urban reserves that indicate where future expansions will take place until 2060. For expansions in the Portland metro UGB prior to the year 2060, the criteria are:

1) Only select IDUs that are adjacent to the existing (or expanded) UGB area.
2) Only select areas within designated urban reserves
3) Select IDUs in order of least equally-weighted distance from: (a) the centroid of the IDU to the center of the UGB area, and (b) the centroid of the IDU to the nearest major road.

After 2060, the Portland Metro UGB is treated like all other UGBs in the WW2100 study area, and expansions take place in accordance with the five criteria listed above.

Allocation of population growth

The developed land value equation includes variables for the population density and household income of the nearest city. As the WW2100 model progresses through time, population and income per capita increase as described above. As the WW2100 model runs, population is allocated on a 5-year basis to UGBs and areas zoned for rural residential (RR) use. No population is allocated to areas outside UGBs and RR areas. For a given increase in a county's population, we use the following procedure to determine the allocation of population to the UGB and RR areas within the county. We begin with the Census block data for 2010 from the U.S. Census Bureau. These data provide a population count for each block, allowing us to determine the initial spatial distribution of population within each county. The block-level estimates are aggregated into a single population count for each UGB and RR area within each

county[1]. Weights are then determined for each UGB and RR area within a county according to their respective share of the 2010 population, disregarding the residual population outside of UGB and RR areas. As the model runs, the increase in a county's population is allocated to the UGB and RR areas according to these weights.

In allocating population to RR areas, we impose a maximum density of one household for every two acres of land to remain consistent with the existing rules governing rural land development. When an RR area as a whole meets this prescribed density threshold, it is shut off from future population growth and its population weight is reallocated proportionally to UGBs and the other RR areas that are still eligible to receive population. We allow household size to vary through time using county-level forecasts in the Woods and Poole data for 2010-2040 and linear extrapolation to 2100.

4.1.5. Land use change validation

The land-use change model is validated in two ways. First, economic theory yields predictions about how net economics returns to alternative uses and other variables should affect land-use decisions. For example, at a given location, a higher return to urban development should increase the likelihood that land in agriculture and forest uses converts to urban use, all else equal. We estimate the parameters of the model using historical data on land-use decisions and hypothesized determinants of these decisions. We confirm that the hypothesized relationships hold in the manner predicted by economic theory. Second, we compared land-use projections from the WW2100 model to historical data. An alternative validation exercise would be to compare land-use predictions from the model to actual data for the same historical period. However, because we estimated the parameters of the model using historical land-use data, such an exercise is not instructive. The model parameters are estimated using maximum likelihood, which guarantees that within-sample land-use predictions will closely match what was actually observed. Ideally, we would compare out-of-sample predictions to observations for the same out-of-sample time period, but, unfortunately, such data are unavailable. Instead, we compare out-of-sample predictions to historical data to ensure that the model is performing as expected. As described below, we compare rates of land-use change for the entire WW2100 model over the period 2010-2100 to rates of change for the historical period 1973-2000.

Table S9 displays a comparison of the land-use model results from the WW2100 reference case scenario with those from the U.S. Geological Survey's Land Cover Trends (LCT) project. The LCT project uses a modified Anderson Level II land-cover classification system, which, combined with the extensive ground-truthing conducted in the LCT project, produces longitudinal land-cover data that more closely aligns with how land is used (in contrast to, e.g., the U.S. Geological Survey's National Land Cover Database, which is based purely on computer-based satellite imagery interpretation) (*43*). Distinguishing land use from land cover is important for this exercise since the WW2100 land-use model mimics human decisions concerning land use, as opposed to changes in land cover that would occur naturally without human intervention. We focus on land development because it is the most common form of land-use change that takes place in the Willamette Basin, both historically and in our model projections. The historical period covered by the LCT data covers 1973-2000, allowing us to

[1] Note that a UGB may span several counties. For example, the Salem-Keizer UGB includes land in both Marion and Polk counties. In such cases, we treat a county's portion of a UGB as a separate area for the purpose of allocating population.

compare the rate of land development projected in the WW2100 model with that of a recent historical period. We provide the comparisons using both the entire WW2100 study area and a refined study area meant to more closely align with the LCT's Willamette Valley (WV) ecoregion. Roughly 98% of the WW2100 land-development decisions, in terms of land area, take place within the WV ecoregion. The vast majority of remaining development takes place on forest land in the foothills of the Cascade Mountain Range.

The results in Table S9 suggest the WW2100 land-use model is relatively conservative in projecting future land development. Over the 90-year period covering 2010-2100, our model predicts that 3.88% (122,378 acres) of the refined study area will be converted from agriculture to development, which compares with 2.40% (85,745 acres) of the WV in the historical 27-year period covered by the LCT data. Similarly, our projected forest-to-development trends appear to be conservative as well, as we predict a conversion share of 1.71% (53,940 acres) compared to the 0.80% (25,452 acres) of the LCT. Given the different lengths of time covered by the WW2100 simulations and the LCT data, one would expect our development shares to be approximately three times larger than the LCT shares. Several factors explain the observed discrepancies. First, the WW2100 land-use model restricts development to occur within urban growth boundaries (UGBs). While the spirit of Oregon's land-use planning system is aimed at confining development to occur within UGBs, empirical evidence suggests development does occur in outlying rural areas (*44*). Second, the WW2100 model assumes growth rates in population and income – key drivers of urban development – than occurred during the historical period. Third, the LCT data is based on a fine-scale grid of 30m land pixels, while the WW2100 data is based on IDUs that range from 5 to over 1,000 acres. The discrete, lumpy nature of the WW2100 units of analysis induces a more restrained pattern of development, as, in reality, there is likely to be fine-scale within-IDU variation in attributes that make some, but not all, of the IDU attractive for development. In the WW2100 model, if the net development returns of the entire IDU do not provide enough of an incentive for the land to be developed, the IDU remains in its baseline agricultural or forest use. Finally, the LCT study area also contains the Vancouver, WA metro area, which experienced some growth in developed area over 1973-2000 that would not be captured in the WW2100 model, which is confined to Oregon.

4.2 Upland forest state transitions

The *Willamette Envision* modeling framework *(1)* was used to simulate annual changes in land cover, vegetation type, and leaf area index *(45)*. *Willamette Envision* relies on a set of State and Transition Models (STMs) for each possible vegetation type. Initial conditions for land cover class, vegetation type, and stand age (if forest) were from Landsat observations *(45)*. These mapping efforts established a network of management-level polygons (Integrated Decisions Units, IDUs). Polygons were an average size of approximately 20 hectares.

The typical sequence of states for a forest STM is from young to mature states differing in age class and leaf area index (LAI). A disturbance, such as harvesting, can reset the successional stage, and vegetation type can shift at that point to an alternative cover type if climate has changed (based on off-line runs of the MC2 biogeography model *(46)*).

The initial rates of forest harvest and wildfire were prescribed based on Landsat observations in recent decades *(47)*. Future rates of harvest in the *Willamette Envision* landscape simulator were the same unless availability of harvest age stands decreased. Future rates of fire were based on the offline runs (using the same climate scenarios) of the MC2 biogeography

model, which has a fire module *(46, 48)*. In the fire module, fire ignition is based on fuel loads (tracked in a biogeochemistry module) and fuel moisture (based on weather). Annual area burned from an MC2 simulation is passed to *Willamette Envision*, and fires are placed randomly on the landscape. Fire size is 22,500 ha except when only a fraction of that is needed to reach the prescribed total area burned.

We assigned a representative LAI to each forest state (i.e. combination of forest type and stand age class) based on off-line runs of the Biome-BGC productivity model *(49)* at WRB sites representative of the different forest types. Biome-BGC is prognostic with respect to LAI and has been run extensively in the Pacific Northwest to simulate forest growth *(50)*. A 25-year daily climate data set from *(51)* was used to initialize the model and run from stand replacing disturbance through the complete range of stand ages. In the Biome-BGC simulations, LAI ranged between 0 and 8 depending on stand age and location, consistent with observations in the region *(52)*. Maximum values were associated with older stands at low to mid- elevations. LAI typically recovered to a value of 2 or more within 10 years of a disturbance and to its equilibrium value around age 20-30.

Each forest state was also assigned a stand height for use in estimating aerodynamic resistance. Again, that was based on stand age. A reference stand age to height relationship is:

$$h = 46.6\ (1 - \ e^{-0.0144AGE}) \qquad (33)$$

where

h = mean height in meters, and AGE = stand age in years.

This equation was constructed from observations of mean stand age and mean height for stands (n= 207) in the West Cascades ecoregion from the USDA Forest Service forest Inventory and Analysis dataset *(51)*.

5. Human water use modeling

5.1 Water rights

Water is allocated in the WRB according to Oregon water law which operates according to the "prior appropriations doctrine" used in most western states *(54)*. The water rights system allocates water according to water right priority date (first date of use historically). Under Oregon law, all water is publicly owned. Irrigators, municipalities or other users must obtain a permit from the Oregon Water Resources Department (OWRD) for a usufructuary right. Under Oregon law, surface or groundwater must be put to a "beneficial purpose without waste." Final certificates of water rights define the timing of use, the maximum rate of diversion, and the annual volume allowed under the water right. When conflicts arise due to shortage, the more senior water right is given priority and more junior water rights are required to curtail their water use if it conflicts with the appropriation of water by the senior water right holder. Water rights may be transferred between points of use under Oregon law when transactions are arranged by parties and approved by the OWRD *(55)*.

Instream flows in the WRB are maintained at prescribed levels in two main ways. State laws that recognize instream water rights as described here are one of these (https://www.oregonlaws.org/ors/537.346). The other mechanism comes from Biological Opinions produced under the U.S. Endangered Species Act for threatened or endangered species. In the WRB there are four threatened or endangered fish species, and minimum flow to support

their habitat are the basis for flow requirements at various control points in the main stem and major tributaries. In general, these are maintained by way of dam operations above these control points: reservoir management rules require the release of water to satisfy the flows prescribed by the Biological Opinion (see section S3.7).

In addition to existing water rights for irrigation, the U.S. Bureau of Reclamation (USBOR) has authority to enter into contracts with irrigators in the basin to supply water from the U.S. Army Corps of Engineers (USACE) reservoirs. Any contract for stored water must also be accompanied by an Oregon water right that specifies the conditions for diverting the stored water released from the reservoir under a given contract (i.e., point of diversion, place of use, use, maximum rate and duty, start date, end date). Currently USBOR is only authorized to offer water contracts to agricultural users *(55)*.

5.1.1 Water rights model

The water allocation model, AltWaterMaster, mimics the process that occurs in reality, namely that when there is insufficient water available to serve the needs of multiple water right holders, the relatively junior water right holders are required to curtail their diversion of water in order to meet the needs of more senior water rights.

The AltWaterMaster algorithm follows these steps on a daily basis: 1) for each POD associated with a water right (surface and groundwater), the algorithm begins with the most senior water right and evaluates whether there is a request for water at that location; 2) if there is a request, the algorithm evaluates whether there is sufficient water available to meet the request, and if there are no other conflicts, the requested amount is diverted and delivered to the corresponding use; 3) if there is insufficient water to meet the requested amount, the request is partially filled with available water, and the remainder is denied. The algorithm identifies the set of water rights upstream from its POD that are requesting water. If there are other upstream water rights PODs that are relatively junior in priority, and if this conflict has been in effect for seven days, then the upstream junior water right is shutoff (for the remainder of the current year) so that the downstream senior water right holder can resume diverting water. For instream water rights, the flow amount required by the water right is maintained in the stream so long as no competing irrigation or municipal water rights are senior to the instream water right *(55)*.

In the case of an instream water right, the amount of water "requested" is the amount provided for as minimum flow for the instream water right. In the case of urban water rights, there is an estimated daily urban water demand (see the Urban Water Demand section). In the case of an irrigation water right, there are three steps for determining the water request for an irrigation water right: i) crop choice, ii) irrigation decision, iii) biophysical water requirements. Depending on the irrigation decision and crop choice outcomes, there will be a soil moisture and crop ET estimated for each day from planting date to harvest date (see section on crop ET). If soil moisture falls below a level adequate to meet the needs of the crop at that particular stage of growth, there will be an "irrigation request" for the amount of water needed to satisfy the crop growth requirements. The computation of the amount of water requested, therefore, depends on human decisions, crop development, temperature and precipitation, and soil moisture and groundwater models.

5.1.2 Water rights model input data

The water rights model requires a detailed input data set to represent the irrigation, municipal, and instream water rights in the basin, with specific details about the locations (point

of use and point of diversion), allowed use, priority date, start date, end date, maximum rates and duties (maximum total annual diverted amount). The input data for the model are based on the Oregon Department of Water Resources (WRD) Water Rights Information System http://www.oregon.gov/owrd/pages/wr/wris.aspx). This data center includes GIS and tabular data for each water right in the state. These data were intersected with the model's IDU parcels and stream layer. Overlaps between POUs and PODs were not exact, but were approximated to achieve a high correspondence between the modeled and the actual existing water rights in terms of size, location and other characteristics. The input data set includes 15,413 irrigation water rights, 1,024 municipal water rights, and 93 instream water rights. Of the irrigation water rights, 8,678 are surface water (232,720 acres) and 6,735 are groundwater (228,800 acres). A parcel of farmland cannot have more than one "primary" irrigation water right (that can be used if there is sufficient water available). The locations of the irrigation water rights are indicated in Figure S3.

Because the vast majority of irrigation water rights in the WRB have identical start dates (March 1), end dates (Oct. 31), maximum rates ($1/80^{th}$ cfs per acre) and duties (2.5 acre-feet per acre), these values were applied uniformly in the model. For municipal and instream water rights, specific rates (max or min) were applied to each water right.

In the case of municipal water rights, most large cities have multiple water rights including surface and groundwater rights, utilizing more than one point of diversion. Use of these water rights is prioritized on the basis of multiple criteria including costs, water quality, and seasonal availability. It is therefore impossible to predict which water right will be used, or used first, based solely on the water right priority date. To replicate the priorities and sequencing observed in the major cities in the basin, water use reports for recent years were used to apportion the urban water demand to the water rights that have been used the most by each city.

The water right sources, types of storage, and forms of conveyance for municipal water supply represent a complex capital-intensive supply system that would be very difficult to accurately model, and to predict in terms of specific decades into the future. Municipalities, for example, buy and sell water among neighboring cities. Portland's main water supply is an out-of-basin source at Bull Run, and the city currently sells about one-third of Bull Run diverted water to other municipalities within the Metro area. The AltWaterMaster model operates on the basis of the expectation that cities within the Portland Metro region will buy and sell water among themselves as needed, and will continue to rely on the major surface water sources used currently. As demand grows, the model allows for additional water to be made available by utilizing sources of water from the mainstem of the Willamette River, which is in fact what is currently being developed by the Tualatin Valley Water District.

5.2 Reservoir operation model

Discharge in the Willamette River Basin is regulated by 13 federally-owned projects that modify the hydrograph to produce the benefits of flood regulation, power production, recreation, fish and wildlife, irrigation, and water quality regulation. The projects were originally constructed with the primary purpose of regulating flood flows, and this operational objective remains the highest priority for determining reservoir releases. The priority of other operating objectives varies by project and circumstance, as described in further detail below.
These 13 projects are jointly operated as a system, not as individual reservoirs. The interdependency of the projects means that changes at any project have impacts on other projects. Reservoir operations modeling is used by the US Army Corps of Engineers (USACE) to analyze the effects of changes on the system. The USACE's Hydraulic Engineering Center

(HEC) developed one of the most commonly applied reservoir operations model (ResSim), which has been implemented in the Willamette River Basin by USACE. ResSim performs rule-based calculations that are constrained by operational goals, regulatory targets, and priorities. The structure of the reservoir operations model (ResSim Lite) implemented within the WW2100 model is based very closely on the 2012 version of the USACE's ResSim model. Specific operating rules and priorities within ResSim Lite duplicate those implemented in the USACE's ResSim model, including the 2009 Biological Opinion flow targets and releases *(56)*.

5.2.1 Operational rules and their implementation

Each reservoir has operational zones (Table S10), which are based on pool elevation on a particular date (Figure S4) and rules sets (Table S11) associated with it. The rule set is prioritized within each zone and across reservoirs, such that the model calculates release quantities and locations (i.e., powerhouse, regulating outlet, and spillway) at each time step to meet the highest priority rule. These rules are organized into a rule priority table for each reservoir, which contains a list of constraints, from lowest priority on top to highest priority on the bottom, for each operation zone within the reservoir. The model attempts to meet all of the priority rules that are physically possible for all reservoirs.

Flows at important downstream locations, henceforth control points, are used to establish releases at reservoirs upstream. Many reservoirs can be influenced by a single control point (e.g Minimum Flow at Salem) and many control points can be influenced by a single reservoir. At any given time step, the system may be in one of three cases:

Case 1: Flow above the maximum. If the flow at a control point is above the maximum allowed (bankfull), then negative amounts are allocated from each reservoir influenced, and outflow is reduced at each of these reservoirs by the specified amount to help bring the control point back within its limits.

Case 2: Flow below the minimum. If the flow at a control point is below the minimum allowed, then positive amounts are allocated to each reservoir influenced, and outflow is increased at each of these reservoirs by the specified amount to help bring the control point back within its limits.

Case 3: Flow is above the minimum and below the maximum. Zero flow is allocated from the influenced reservoirs.

In addition to flood regulation at control points, a number of other constraints are implemented within the modeled and actual system. For example, environmental flow targets were established under the 2008 Willamette Project Biological Opinion *(56)*, as indicated in Tables S12 and S13. The April-October flow targets vary based on the type of water year (Table S14). The water-year type is established in the WW2100 model on 20 May, when the volume of water stored in all of the reservoirs is summed.

Within the WW2100 model, each reservoir has one data object that stores eight variables: time, pool elevation, rule curve elevation, inflow, outflow, powerhouse flow, regulating outlet flow and spillway flow. The combined set of rules, constraints, priorities, and current conditions are queried at each time step to establish releases, as summarized in the following series of functions:

1. *Update elevation and rule curve information and set desired release.* The current pool elevation is obtained and maximum gate outflows are updated based on the current pool elevation. If the reservoir is a re-regulating reservoir (used to smooth releases from an

upstream reservoir), inflow is set equal to outflow and the rule process is skipped. The desired release is the amount of water needed to be released to take the pool elevation back to the target pool elevation in one timestep. If a reservoir is below the target pool elevation, then the desired release is set to 0.

2. *Define the operations zone.* The operations zone defines which rules are to be used to determine outflow. The operation zone is defined by the current pool elevation with respect to the rule curve (conservation curve in Figure S4). Once the operating zone is determined, constraints are applied in order, determined by their place in the rule priority table.
3. *Apply constraints, prioritized within each zone.* Constraint values are obtained from lookup tables for each individual rule. If the constraint value applies (e.g. the outflow is greater than a maximum, less than a minimum, etc.), then the actual release is adjusted to conform to the constraint. The constraints are applied in order of priority, from lowest to highest. The logic describing release decisions is explained in detail in *(57)*, Section 11.4.1 of the HEC-ResSim User's Manual. A number of constraints may be implemented in any given time step. Max and Min constraints set upper and lower boundaries on outflow. Increasing rate and decreasing rate rules govern the allowed rate of change of flow releases (ramping rates). The control point constraints adjust outflow based on current conditions at the control point. After application of all the rules, outflow is checked to see if it is below the allowed minimum flow. Each time a constraint changes the outflow value, the name of the constraint is stored as the "active rule." The final constraint applied, and thus the constraint controlling the outflow value, is stored for output.
4. *Assign Reservoir Outlet Flows.* Once the outflow for a particular reservoir has been determined, the outflow is split between the outlets, which can be power plant outlets, regulating outlets, or spillway gates. Outlet are subject to physical and operational constraints, and all the reservoirs in the model are prioritized in the same way, with outflows being routed first to the penstocks for those that have a powerhouse, followed by regulating outlets, and finally to the spillways.

The following values are collected at each time step (daily) for each reservoir modeled for display in *Willamette Envision*: Pool Elevation, Rule Curve Elevation, Inflow, Outflow, Powerhouse Flow, Regulating Outlet Flow, Spillway Flow, and the active rule, described in step 4 above.

5.3 Urban Water Use Models

5.3.1 Overview

The urban water use models consist of demand relationships for residential and nonresidential urban water use for four major urban areas in the Willamette basin: the Portland metropolitan area, Salem, Corvallis, and Eugene – Springfield. Additionally, there is a separate model that combines residential and non-residential demand for smaller urban areas. These demand relationships are used to generate estimates of the quantity of water used in each urban area in future decades. The variables included in these models were selected based on a review of the economics literature on urban water demand. An additional consideration was the need to use variables that could be forecasted over the entire study period, either as exogenous drivers

(such as income and population growth) or as variables generated by other models within the *Willamette Envision* framework (such as population density).

5.3.2 Methods

The economics literature on urban water use indicates that water demand is a function of the marginal price of water, pricing structure, income, and weather and seasonal effects *(58-62)*. Additionally, given the specific forecasting needs of the urban water component, we included population and population density in the model. The model of residential water demand therefore predicts total daily water used by residential customers (in hundreds of cubic feet – ccf) as a function of price ($/ccf), pricing structure (increasing block rate or flat rate), city population, median household income, and population density (persons/mile^2). The model of nonresidential water demand predicts total daily water used by nonresidential costumers (in ccf) as a function of price, total city industrial (manufacturing) income, total city commercial income, and population.

The values of the response parameters for these variables were obtained from the economics literature:

- Long-term price elasticity of demand: -0.6 *(60)*;
- Income elasticity: 0.13 for flat rate pricing, 0.18 for increasing block rate pricing *(58)*;
- Population: 1.0 *(63)*;
- Population density: -0.048 *(64)*;
- Industrial (manufacturing) income: 0.11 *(61)*;
- Commercial income: 0.04 *(61)*.

We collected the most current information available at the beginning of the project for each of these variables for Portland, Salem, Corvallis, Eugene, and Springfield. Information on water rates, price structure, and water use was obtained from Water Management and Conservation Plans for Portland (2010), Salem (2009), Corvallis (2005), and Eugene (2012), and from the Springfield Utility Board Springfield (2012). Information on personal, manufacturing, and commercial income comes from the Bureau of Economic Analysis. Population and population density information is from the US Census. The coefficients listed above were combined with the averages of water quantity, price, income, population, and density for the five cities to calibrate a log-linear model and calculate the intercept term corresponding to the baseline averages. Because the intercept varies with the pricing structure, we calculated two intercepts using the corresponding averages for cities with flat rate and increasing block rate (IBR). Then we calculated the necessary coefficient for the IBR indicator variable to give the correct intercept when IBR is set to 0 or 1. Finally, the demand models were adjusted to reflect seasonal variations in demand.

The resulting models for the four main cities (Portland Metro, Salem, Corvallis, Eugene-Springfield) are as follows.

Residential demand:

$$\ln(Q^R_{Avg}) = -(3.0159618 + 0.47698\,IBR) - (0.6\ln(p)) + \ln(Pop) + (0.13 + 0.05\,IBR)(\ln(I)) - (0.048\ln(D)) \quad (34)$$

$$Q^R_t = \exp(\ln(Q^R_{Avg})) \text{ [units are in ccf/day]} \quad (35)$$

Non-residential demand:

$$\ln(Q^{NR}_{Avg}) = -2.727616 - (0.6\ln(p)) + (0.11\ln(Ind.I)) + (0.04\ln(Comm.I)) + (0.85\ln(Pop)) \quad (36)$$

$$Q^{NR}_t = \exp(\ln(Q^{NR}_{Avg})) \quad (37)$$

where Q^R and Q^{NR} are the sum of the total daily water use for the entire city in hundreds of cubic feet (ccf), p is price in $/ccf, Pop is city population, D is density (persons per square mile), I is median household income, IBR = 1 if the city has an Increasing Block Rate pricing structure and IBR = 0 otherwise, *Ind. I* is total city industrial (manufacturing) income (thousands of $), and *Comm. I* is total city commercial income (thousands of $).

For other cities, demand is also a function of population, income, and price ($/ccf). They do not have separate non-residential demand functions, nor do they use IBR pricing. Prices are based on the water delivery average cost function, which declines with rising population.

We adjust residential demand above for seasonality by decomposing daily water use into outdoor and indoor use components, based on twenty-four years of daily data from Portland Water Bureau. Total predicted yearly water demand from above is divided by 365 to obtain daily use, and then multiplied by indoor and outdoor fractions to reflect seasonality. Outdoor water use rises from a negligible share of daily use between November and April to a maximum of 43% of daily use in late July.

The baseline prices used for calibration for the four main cities are:
Residential: Portland (all of metro area): $2.44/ccf, Salem: $2.04/ccf, Corvallis: $1.93/ccf; Eugene-Springfield: $2.00/ccf.
Non-residential: Portland (all of metro area): $2.44/ccf, Salem: $1.50/ccf, Corvallis: $2.11/ccf; Eugene-Springfield: $2.00/ccf.

We set IBR = 1 for Corvallis and Eugene-Springfield, and IBR = 0 for Portland, Salem. We use IBR = 0 for other urban areas.

Baseline manufacturing income (x 1000 $) is 9,851,720 for Portland, 651,857 for Salem, 461,476 for Corvallis, and 723,165 for Eugene-Springfield. Baseline commercial income (x 1000 $) is 58,292,148 for Portland, 7,350,692 for Salem, 1,598,343 for Corvallis, and 6,565,399 for Eugene-Springfield.

Rural residential demand is given by

$$\ln(Q^{RR}) = -3.55 - (0.6 \ln(PC)) + \ln(Pop) + (0.13 \ln(I)) - (0.048 \ln(D)) \quad (38)$$

where PC is the "price" for water ($/ccf) (the cost of pumping, $0.3/ccf), Pop is the population of the rural residential IDU, I is average income per household for the relevant county, D is density (people per sq. mi.) (assumed to be 768 per square mile in rural areas, or two acres per household).

Future water price trends are highly uncertain. We set up a base case path for water prices that allows for increases of 6% each year from 2011 to 2015 to reflect price increases observed in several urban areas in the study region since 2010. Additionally, we implement an average increase in water prices of 1.5% per year from 2016 to 2025 based on evidence of rising financial needs for many water utilities in the basin due to a backlog of infrastructure maintenance needs as well new capital requirements for expanded capacity and seismic risk reduction upgrades. Beyond 2025 prices are assumed to change in proportion to average current cost (AC_t), which is a function of population. Sensitivity analysis on this base case price path was performed for 25%, 50% and 75% higher priced trajectories, indicating demand growth up to 30% below the baseline levels.

Specifically, the following relationship was estimated using national data *(63)*:

$$AC_t = 0.748 \exp\{9.93 - 0.355 \ln Pop_t + 0.030(\ln Pop_t)^2 - 0.001(\ln Pop_t)^3\} \quad (39)$$

Prices change according to

$$\frac{P_t - P_{t=0}}{P_{t=0}} = \frac{AC_t - AC_{t=0}}{AC_{t=0}}; P_t = \frac{AC_t}{AC_{t=0}} \times P_{t=0} \ . \quad (40)$$

5.3.3 Validation

We conducted two validation exercises for the urban water demand model. First, we compare the predicted per capita water consumption calculated from the model with values reported by the corresponding city utilities. Table S15 suggests that the model predicts per capita water use for 2010 reasonably well, both on average and for individual urban areas. The model estimate for per capita consumption for 2010 is somewhat lower than the observed levels. This reflects in part the rising prices and declining trend observed during this period.

Second, we used the urban water demand model and data on water prices and water consumption for Portland from 1995 to 2011 (from Portland Water Bureau) to generate a hindcast of water consumption in Portland during that period. The objective is to compare water consumption predicted by the model with observed data, given the relatively large price increases over the period, as shown in Table S16. The average yearly increase in water use was 5.3%. The table shows the water use predicted for Portland by the model, along with observed consumption amounts. The trends are show in Figure S5.

Per capita water use decreased by 39.83 gallons per day (26%) between 1994 and 2012. For that period our model predicts a total decrease of 39.84 gallons per day (31%). Hence, this "precasting" exercise suggests the urban water model replicates trends in per capita water consumption in response to changes in water price well[2].

5.4 Agricultural water use

In each year that an IDU is assigned to the agricultural land use, farmer decisions are modeled to simulate crop choices and irrigation decisions. Irrigation is only possible on IDUs with existing irrigation water rights. These initial decisions are then followed by daily decisions related to planting and harvesting, and (possibly) applying irrigation water. The availability of irrigation water is also subject to regulatory shutoffs in accordance with the prior appropriations seniority system under state law (as described in S5.1). These combinations of decisions, choices, actions and responses to exogenous factors produce a unique pattern of crop water use, irrigation diversions, soil moisture and groundwater contributions, and net farm income (annual land rent) at the IDU level. To the extent that irrigation water is shutoff by regulators, short-run annual land rent is reduced, as is long-run (expected) land rent.

Crop water use in agriculture is estimated on a daily basis reflecting the crop or vegetative cover of each IDU and evapotranspiration as a function of meteorological factors, crop type and growth stage (as described in S3.6). If a field is irrigated, the amount of water diverted and applied to a field will exceed this biological crop water demand to reflect the average irrigation efficiency of the application and conveyance technologies used in the basin (primarily sprinkler irrigation). An irrigation efficiency of 0.8 is assumed, so that the applied water will exceed crop requirements by 25%. The extra water not accounted for by crop ET is returned to the soil and subsurface reservoirs, and ultimately back to the stream network.

[2] Note that the model is not intended to predict water consumption in Portland individually, as it is calibrated using data for the five major urban areas in the basin.

5.4.1 Crop choice

The crop choice model estimates the probability of growing each of seven crop types or groups for the modeled year. The empirical model is estimated at the parcel level based on observed cropping patterns in recent years. The model estimates the crop observed as a function of IDU characteristics including soil quality (land capability class), elevation, and the presence of an irrigation water right, as well as varying attributes including crop prices and expected water availability (for those IDUs with irrigation water rights). Given the estimated probabilities for each IDU, the simulation models determines the crop for each IDU in each year with a random draw reflecting these estimated probabilities. No evidence of crop choices being correlated across years (i.e., a crop rotation schedule) were found in the data or in interviews with farmers or agricultural extension personnel. Crop prices are assumed to remain constant (in real terms) in modeled scenarios given their high uncertainty.

The crop choice model is estimated as a hedonic relationship based on parcel-level GIS data on 100,555 parcels over a six year period. Crops were identified using USDA Crop Scape agricultural land cover data. Parcel data included land characteristics (land capability class (LCC), elevation, slope, field size, and water rights), climatic characteristics (average precipitation, minimum temperature), and crop prices.

The model was estimated using ordinary least-squares as follows:

$$P_j = \beta_0 + \sum_{i=1}^{14} \beta_i \qquad (41)$$

for crops j = 1 to 8 where 8 is "other crops," where P_j is the probability of planting crop j in the current year, and independent variables 1-14 are:

LCC_1 to LCC_7 = the dominant soil type (land capability class) in the IDU
EL = elevation (in meters, demeaned where $\overline{EL}$= 97.2)
SL = slope (percent) (demeaned, where $\overline{SL}$= 3.704)
PR = precipitation April-October (inches, demeaned where $\overline{PR}$ = 13.63)
MT = minimum temperature April-October (degrees C, demeaned where $\overline{MT}$ = 8.556)
PG = price of grass seed (average over period = \$64/ton)
PW = price of wheat (average over period = \$5/bushel)
IR = existence of irrigation water right (1 if a water right exists, otherwise 0)

The estimated coefficients are indicated in Table S17.

The resulting modeled values are interpreted as the probabilities for each crop to be grown. The model is implemented as a "random draw" to determine which crop is grown each year at a given IDU location. The effect of the existence of an irrigation water right on crop choice will be moderated to the extent that a water right shutoff is anticipated in a given year. To represent this circumstance, the implemented crop choice model included an additional term, $IR*SE$, the interaction of IR as defined above with SE (expected snow), where SE = 1 if the April 1 snowpack measure is greater than or equal to the average snowpack in the previous 10 years, or SE = (1- SH) if the April 1 snowpack measure is less than the average snowpack in the previous 10 years (and where SH = the frequency in the previous 10 years that the water right has experienced a regulatory shutoff ($0<SH<1$, with an initial value of 0 for all IDUs).

For perennial crops (orchards, vineyards, tree crops), a fixed set of IDUs is permanently assigned. These areas represent a relatively small proportion of farmland in the basin; they are relatively stable in area and location.

5.4.2 Irrigation decisions

Farmers in the WRB typically own and cultivate multiple fields and each year make decisions about which crops to grow on each field, whether to irrigate those field with irrigation water rights, what equipment to use on which fields, etc. We model these decisions at the parcel (or IDU) level as representative of farm-level decisions. A survey was conducted in the fall of 2012 to collect data from farmers' about their irrigation and crop choice decisions for a sample of parcels, and over the previous six years for those individual fields. The survey had a unique design in that farmers were asked to identify their irrigated fields on a map, so that their responses could be matched to land quality and climate data. Integration of survey responses with spatial data allowed for development of an irrigation decision model that could explain why a large percentage of existing water rights were not being used in a given year.

A sample of 530 farmers were surveyed and data was collected on up to three fields for each farmer over a six year period. A discrete choice irrigation decision model was estimated based on these data *(71)*. The logit model estimated takes a form such that the probability P_{IR} of irrigating a given field is estimated. Using a panel of 4,409 observations the following relationship was estimated:

$$\ln\left(\frac{P_{IRR}}{\left(1-P_{IRR}\right)}\right)=\beta_0+\sum_{i=1}^{17}\beta_i x_i \qquad (42)$$

where the variables and their estimated coefficients are indicated in Table S18.

The spatial data sources include PRISM data for monthly precipitation April to August (2007-2012) as well as for 30-year monthly averages (1980-2010); the soils gridded data (10 meters) and elevation data came from USDA GeoSpatial Gateway. Water rights were from the Oregon Water Resources Department. Distances to major cities and to the Willamette River were computed using Oregon GIS clearinghouse data on streams and city boundaries. Soil water holding capacity comes from the Arc GIS SSURGO layer.

Crop choice and irrigation decisions are interdependent. Farmers may make crop choices and irrigation decisions simultaneously or, if sequentially, in either order. In the WRB most major crops are sometimes grown non-irrigated or irrigated. The correlations in these decisions are reflected in the crop cover data, irrigation survey data, and are reflected in the crop choice probabilities. In addition, farmland rent reflect profits from farming and irrigation decisions. In general farmers will not plant or irrigate land that is expected to generate no profit or rent. Reflecting this, the following rules were introduced in the simulations:

i. If farmland rent < $1, crop choice is fallow and probability of irrigating = 0.
ii. If the irrigation decision is 'yes', the probability of fallow is zero.
iii. If the irrigation decision is 'yes', the probability of wheat is zero.
iv. If the irrigation decision is 'no', the probability of corn is zero.

As a result of these adjustments for fallow, wheat, and corn, the probability of "other crops" (j=8) is adjusted for consistency so that $P_8=1-\sum_{j=1}^{7}P_j$.

Although irrigation can increase profits through higher yields and by expanding the range of crops that can be grown, it is also costly in time, energy costs and capital costs. Since farmers are heterogeneous in their production skills and in the attributes of their land, the additional benefits will justify irrigation for some farmers but not for others, and in some years but not in other years.

5.4.3 Farmland rent

The economic rent or annual profit from farming a given piece of land can play an important role of farm decisions to plant a crop, irrigate, or transition out of farming. Our estimation of farmland rent takes a Ricardian approach that is common in models of the economic returns to agriculture *(72)*. Land value is assumed to equal the net present value of future rents from putting the land to its highest value use; as a result we expect to see variation in land values and annual rents due to characteristics of the land that would influence agricultural productivity such as soil quality and precipitation or irrigation water rights.

Similar to the hedonic model of crop choice, farmland rents are decomposed as a function of the factors affecting agricultural productivity *(71)*. The source data on farmland values and rents originate from data collected by county assessors, a process required in Oregon to monitor levels and trends in both real market land values and assessed values. Drawing on land sales, land rentals, surveys, and expert analysis, county assessors produce estimates of average farmland rents within a county by soil type, or Land Capability Class (LCC) and by zone within a county, for parcels with and without irrigation water rights. In the absence of an adequate sample of data on individual farmland sales, these semi-aggregated data reflected sufficient variation across zones and soils that hedonic analysis could be used to infer the contribution of other covariates such as elevation, precipitation, minimum temperature, etc. The first step was to assign a rent to each parcel across zones, soils and water right assignments according to the county estimated real market value for those locations and characteristics. These became the dependent variables for a hedonic model estimation that included two variables that determined the assigned rent level (LCC and existence of irrigation water rights), as well as other characteristics of the parcels (elevation, temperature, precipitation, etc.). By regressing these variables on the farmland rent estimate, we are able to recover, for example, the marginal value of higher summer temperature or lower elevation independent of the soil class.

To compile a data set of agricultural tax lots spanning the extent of the Willamette Valley, cadastral and zoning tax lot data were collected from all counties, identifying the tax lots zoned for agricultural use. Small tax lots less than 10 acres were excluded. See (71) for additional detail. The hedonic estimation included soil classes *LCC* 1-4, 6, and 7 independently, and in the case of *LCC* 1-4 interacted with a dummy variable for existence of an irrigation water right (*IRR*).[3] Independent variables include the IDU elevation, historical average growing season precipitation (demeaned using the basinwide mean), historical average growing season minimum temperature (demeaned using the basinwide mean). Parcel size in acres was interacted with each of elevation, precipitation, and temperature. For the IDU values of farmland rent, mean parcel size was assumed.

Using these data the rent for each parcel was estimated with the following form:

$$R = \beta_0 + \sum_1^{16} \beta_j X_j + \varepsilon \qquad (43)$$

where R is the parcel rent (per acre per year), β_0 is the intercept, X_j represents the variables in the Table S19 where the estimated coefficients are shown for each of the 16 variables, X_j.

The long-term farmland rent denotes the expected rents *E(R)* in future years based on recent observed rents, including the potential risk associated with shutoffs of irrigation water rights. With the short-term economic rent estimations above, and the updated modeled values for

[3] There were insufficient observations of LCC5 land in the data to estimate a coefficient. As a result, we have assumed LCC5 lands will be treated as if they have the same value as LCC6 lands.

shutoffs, the value of *E(R)* is estimated annually by interacting the four irrigable LCC variables with a measure of the risk of an irrigation shutoff (*SH*), where *SH* in year *t* equals the frequency in the previous 10 years that the IDU's water right had been shut off ($0<SH<1$; initial value $SH=0$).

The farmland rent data as well as farmland sales data indicates a relatively low value of irrigation water rights (averaging $17/acre-foot of applied water) compared to other irrigated areas in the western U.S. These lower values for irrigation water reflect the relatively high precipitation in the Willamette Valley during spring and early summer in most years. There is sufficient rainfall leading up to and over the course of the growing season that irrigation is not essential for many crops. As a result, a proportion of irrigation water rights go unused in any given year. Indeed, the area of land irrigated in a given year in the Willamette Basin (based on the USDA Census of Agriculture) is about one-third less than the area possessing irrigation water rights *(68)*.

The distribution of irrigation water rights in the basin, and the realized or potential economic rent (incremental profits) from irrigation were estimated for each IDU in the valley (see Figure S3). The location of the farmland without water rights, and their distance to a river below one of the federal storage dams, is critical for determining whether water could be conveyed to these farmlands at a cost that would be economic. See section S5.4.5.

S5.4.4 Validation

The combination of model results for crop choice, irrigation decisions, and farm rents are compared here with data from the USDA Census of Agriculture, 2012 (Table S20). The main crop categories among harvested cropland acreage in the USDA data are grass seed (53%), hay (15%), orchards (5.6%), vegetables (included as "other") (5.4%), field crops (4.5%), and nursery crops (4%), also included in Table S20 as "other"). This pattern has been relatively stable for many years for the major crops; grass seed has been the dominant crop by acreage for more than 50 years.

Harvested cropland has averaged about 900,000 acres over the past decade, declining from a high of about 1 million acres in the 1980s. About 267,000 of these acres, or about 30%, are irrigated in any given year (USDA Census of Agriculture data, 1997-2012). Of these, just over half (about 140,000 acres, or 52%) are irrigated with surface water rights. The breakdown between surface and groundwater irrigation is based on our own farm survey (discussed above under "Irrigation decisions").

The acreage of irrigated farmland in the Basin has remained relatively stable since the mid-1990s. Prior to that time, irrigated acres rose gradually, reflecting the acquisition of new irrigation water rights. Since the available live flow water rights were fully allocated as of the 1990s, no new irrigation water rights have been approved by the OWRD.

Data on existing irrigation water rights indicate about 462,000 acres with irrigation water rights from surface, groundwater, and stored water (federally contracted) sources. Given the annual irrigated acreages of 267,000 acres, this indicates a rate of utilization of irrigation water rights of 55 to 60%. The estimated frequency of utilization of irrigation water rights from our farm survey (and the basis for the modeled acreages irrigated) was 62%.

An exact count of irrigation water rights is complicated by several factors: (a) Water rights can sometimes have multiple uses (irrigation, domestic, livestock); (b) A small fraction of irrigation water rights in the WRB are "supplemental water rights" rather than primary, and thus cannot be used unless the primary right is exhausted or unavailable (supplemental water rights

were not included in this model); (c) The Oregon water rights database contains measurement errors, GIS errors, and other imperfections; and (d) some water rights may have been abandoned or are not known to the landowner.)

5.4.5 Conveyance costs for new irrigation

The annual economic profitability estimates for farming with and without irrigation water rights is estimated above in S5.10. These results reflect both the additional costs and added revenues that come with irrigation, on average for the sample locations, soil classes, and types of irrigation infrastructure observed. The number of farms with irrigation water rights in the basin has been stable since the 1990s.

Agricultural lands in the Willamette basin that currently do not have irrigation water rights may benefit from opportunities to acquire new water rights under federal contracts for stored water at one of the USACE reservoirs. An important question surrounding this large volume of stored water in federal reservoirs (1.6 million acre-feet) is whether farmland that currently does not have irrigation water rights could switch from rain-fed agriculture to irrigated agriculture profitably. Most existing irrigation relies on surface water or groundwater sources very near or within the parcels being irrigated. In the case of stored water from federal reservoirs, the water would need to be transported from a river that is downstream from one of the federal dams to a currently unirrigated field. The costs of conveyance for this option may be significantly higher than for existing irrigation. Costs will vary by distance and lift (raising the water through pipes above the level of the river). Large scale canals that rely on gravity and serve large areas of farmland are no longer possible because creating the necessary right-of-ways along topographical gradients now conflict with a multitude of private properties, roads and other infrastructure. Recent developments of new irrigation in the basin have involved underground pipes and pumps. The costs of these same technologies are estimated here.

The profitability of a new contract for stored water will depend on a comparison of the irrigation benefits (higher yields and wider range of crop choices, estimated as described above in 5.4.2) and the additional costs (capital investments in infrastructure, labor, and energy costs). For new contract water rights we assume the irrigation premium to be the same as for existing irrigation water rights if the costs of irrigating are similar to the average costs for existing surface and groundwater rights. In the case of new water rights from stored water we expect the costs to be somewhat higher due to a) the fee paid to the BOR for the water contract, b) the extra cost for mainline conveyance to bring the water from a below-reservoir tributary to the field, and c) the extra lift required. Whether or not a new irrigation water right will be attractive to a farmer will depend on whether farming with irrigation is more profitable than without irrigation.

One of the alternative scenarios used in the analysis for this paper involves allowing currently non-irrigated farmlands to adopt irrigation relying on stored water contracts if increase in revenue exceeds the increased costs. Changes in revenues will vary by soil class; changes in costs will vary due to the distance and lift required for water conveyance.

The estimate of these costs are described here. There are two components to these costs, a) the infrastructure and installation capital costs and b) the additional energy costs. For both of these costs we estimate average values for a representative irrigation operation of 120 acres (which could involve combining multiple fields via cooperation or land sales).

Capital costs for mainline conveyance systems include the pipe and below-ground installation costs. The size of the pipe is tied to the flow rate needed to serve the irrigable area; larger pipes are more costly but also increase capacity and reduce friction losses. For a range of

diameter pipes the costs, capacity, friction losses and irrigable areas are shown in Table S21. Our analysis is based on use of an 8" pipe to serve a 120-acre farm. The annualized capital costs are estimated to be $0.59 per year per 100 feet of mainline (assuming 120 acres, or an average rate of 6.5 gpm). So for a mainline of 1,000 feet, this would mean an added cost of $5.90 per acre per year. In addition, there is a charge from the US Bureau of Reclamation that will average about $9/acre.

The extra variable costs for irrigation with a stored water irrigation contract are energy costs for pumping water a given distance and lift along the mainline pipes to bring water from the point of diversion from a river to the irrigated field. The added cost is estimated as a function of the mainline length and the lift *(73, 74)*.

The energy cost, *c*, can be expressed as

$$c = p \times E \tag{44}$$

where *p* is the price of electricity ($/kwh) and *E* is the energy consumed in kwh. We have

$$E = t \times (output\ \ power) \tag{45}$$

where *t* is time (hours) and *output power* is the power per unit time. The rate of energy use is

$$output\ \ power = \frac{q \times TDH}{3{,}960} \tag{46}$$

where q is the pumping rate per hour, and TDH is the total dynamic head, or the sum of the lift, head losses, friction losses, and the pressure at the pump (in psi multiplied by 2.306 to get horsepower).

To convert output power from horsepower to kilowatts we multiply by 0.746. And to adjust for the overall pumping plant efficiency, E_{plant}, the expression is divided by this value, which can range from 0.7-0.8. A midrange value for pumping plant efficiency is 0.75, or input power must be one-third higher than output power.

The hours of pumping, *t*, necessary to apply the required irrigation water (acre-inches), *d*, is computed as

$$t = \frac{(d \times 27{,}154)}{(q \times 60)} \tag{47}$$

Combining the relationships in (2), (3) and (4) above and simplifying (e.g., 27,154/(60*3960)=0.114285) we can write this as

$$c = p\left(\frac{d \times TDH \times 0.114285 \times 0.746}{E_{plant}}\right) \tag{48}$$

For our benchmark assumptions we use p=0.06, d=16 inches/acre, and E_{plant} = 0.75.

To estimate the incremental energy costs for the length and lift of additional mainline systems, we need to compute the additional TDH due to the additional mainline length and lift.

The Hazen-Williams formula for head loss in a pipe is:

$$H_f = K\frac{\left(\frac{Q}{C}\right)^{1.852}}{D^{4.87}}(Length) \tag{49}$$

where H_f is friction head loss (feet/foot), Q is flow rate (gpm), D is the inside diameter of the pipe (in), K_f is a constant (1046), length is the length of the pipe (feet), and C is a "roughness factor."

For a representative system in the Willamette basin we will assume C=140 (for PVC pipe), Q=672 gpm (5.6 gpm for 120 acres), D=8 inches. With these assumptions we can estimate

H_f as a function of the length of the pipe. To this we add the required lift (in feet) to get the portion of TDH attributable to the extra mainline conveyance. With these parameters, the additional cost for mainline conveyance is estimated to be $0.069/per acre for every 100 feet of mainline, and about $0.091/acre for every 10 feet of lift.

Total additional costs with stored water contracts

Combining these fixed and variable cost estimates on an annualized, per acre basis, we get the following costs per 100 feet of mainline: $9 (contract price), plus $0.59 (capital cost), plus $8.35 (energy cost). To this add $0.11 per foot of lift. For a parcel that is 300 feet from the below-reservoir stream, and 20 feet above the stream, the extra conveyance cost would be $36.80 per acre per year.

Two versions of an alternative scenario allowing adoption of new irrigation water rights tied to stored water contracts were run. The first of these included these added costs for all parcels currently without water rights. In cases where the estimated increased farm rents exceeded the additional conveyance costs, the probability of adoption rose as a function of the increased profits per acre. Probabilities were sufficiently high so that all profitable adoptions occurred by the year 2030. In the second version of this "new irrigation" scenario, the costs of conveyance were reduced by half, and the fee paid to the USACE was eliminated. The areas adopting new irrigation rose under the second scenario, but remained below 30,000 acres of newly irrigated land.

6. Model scenarios, sensitivity analysis, and validation

The WW2100 model simulations for the period 2010-2100 include a reference case or "business-as-usual" scenario as well as 21 alternative scenarios (see Figure S6). This reference case scenario includes mid-range assumptions about climate change, population and income growth, and also includes assumptions about prices, institutions, and other parameters in ways that represent the most likely future conditions. These maintained assumptions include water rights, the Oregon land-use planning system, reservoir operating rules, forest practices, and urban water prices. The descriptions above for the climate model, population and income trajectories and other assumptions are those used in the reference case scenario. Many aspects of the scenarios were developed and refined working closely with a wide range of stakeholders.

The other 21 alternative scenarios were modeled and run for a variety of purposes including sensitivity analysis, counterfactual comparisons with the reference case, and validation (for example, simulating the 1950-2009 historical period and comparing the hydrology to measured results). The other scenarios varied climate change, population and income growth, reservoir operations, urban expansion, forest fire suppression, irrigation and cropping decisions, implementation of additional planned instream flow water rights, and resource management decisions. Sensitivity analysis scenarios included the use of either the reference case or the high climate models described in S2.1. Population and income growth were modified to generate alternative scenarios for a doubling of the population growth rate. In addition to this, counterfactual scenarios were run for a) no growth in income, b) no growth in population, and c) no growth in either population or income.

The scenarios implemented as sensitivity analysis, as well as the modeling of the historical period, represented one way to assess the effects of multiple sources of uncertainty in the model. Additional scenarios in the study include a) changes in reservoir management

(delayed refill of reservoirs during the spring; and "run of the river", e.g., no filling of reservoirs), b) no agriculture, c) changes in the propensity to irrigation (higher, lower), d) less restrictive urban growth boundary expansion, e) increased wildfire suppression, f) new irrigation water rights linked to reservoir storage of water, and g) additional instream water rights (as are currently in the process of being implemented by the state of Oregon).

Fifteen of the scenarios modeled, including the reference case, provide a basis for evaluating the sensitivity of model outputs to a range of assumptions reflecting uncertainty about future patterns or trajectories. These include uncertainty about climate change, population growth, income growth, future policies such as land use regulations, irrigation water use, the implementation of new regulations for instream flows, or combinations of the above. Taken together, these scenarios that modify one or multiple changes in these assumptions provide a measure of the variability in model outcomes resulting from these alternative assumptions. The set of metrics in Table S22 include the standard deviation and coefficient of variation for a set of modeled outcomes related to water supply and demand. The mean CV is 9.2%. Given the wide variation in assumptions for some of the scenarios (e.g., high climate change, doubling of population growth, much higher irrigation rates) this level of variation seems modest. In several cases, relatively high CVs are obviously due to several of the scenarios (e.g., snow evaporation across climate scenarios). When small numbers of these specific scenarios are excluded, the CV is much lower. Using these subsets as indicated in Table S22 reduces the average CV to 2.7%. Validation and verification of model components was undertaken in a variety of ways, depending on the model type and other factors. As described above, climate models were chosen to provide a close fit to historical data (section 2.1). Hydrology models underwent detailed calibration (section 3.7). Land use change, urban water demand, and agricultural cropping and irrigation were each compared to historical patterns and were found to be validated (sections 4.1.5, 5.3.3, and 5.4.4, respectively). Undertaking a whole-model validation exercise was not feasible because it would require ascertaining a new set of initial values (e.g., for year 1980) for the attributes on all 165,000 IDUs (i.e., land use, land value, forest inventory, water rights, urban growth boundaries, as well as water prices, population and income parameters), an effort for which adequate data and documentation do not exist.

SI Appendix References

1. Envision. http://envision.bioe.orst.edu/ (2014).
2. US Geological Survey (USGS). National Hydrography Dataset. Found at http://www.horizon-systems.com/NHDPlus/NHDPlusV2_home.php (2014).
3. J. E. Halofsky, M. K. Creutzburg, M. A. Hemstrom. Integrating social, economic, and ecological values across large landscapes, General Technical Report PNW-GTR-896. U.S.D.A. Pacific Northwest Research Station (2014).
4. ILAP. Integrated Landscape Assessment Project. http://oregonstateedu/inr/ilap (2013).
5. R. E. Kennedy, Z. G. Yang, W. B. Cohen. Detecting trends in forest disturbance and recovery using yearly Landsat time series: 1. LandTrendr—temporal segmentation algorithms. Remote Sens Environ 114:2897–2910 (2010).
6. R. E. Kennedy, Z. Q. Yang, W. B. Cohen, E. Pfaff, J. Braaten, P. Nelson. Spatial and temporal patterns of forest disturbance and regrowth within the area of the Northwest forest plan. Remote Sens Environ 122:117–133 (2012).
7. J. L. Ohmann, et al. "Mapping change of older forest with nearest-neighbor imputation and Landsat time-series." Forest Ecology and Management 272: 13-25 (2012).
8. USGS, National Gap Analysis Program (http://gapanalysis.usgs.gov/, 2014).
9. D. E. Rupp, J. T. Abatzoglou, K. C. Hegewisch, P. W. Mote. Evaluation of CMIP5 20th century climate simulations for the Pacific Northwest USA. Journal of Geophysical Research-Atmospheres 118:10884-10906 (2013).
10. J. A. Vano, J. B. Kim, D. E. Rupp, P. W. Mote. Selecting climate change scenarios using impact-relevant sensitivities. Geophys. Research Letts. 42.13: 5516-5525 (2016).
11. J. T. Abatzoglou. Development of Gridded Surface Meteorological Data for Ecological Applications and Modelling. International Journal of Climatology 33:121–131 (2012).
12.S. Bergström,V. P. Singh. "The HBV model." Computer models of watershed hydrology. pp. 443-476 (1995).
13. S. Bergström, B. Carlsson, B., M. Gardelin, G. Lindström, A. Pettersson, M. Rummukainen. Climate change impacts on runoff in Sweden assessments by global climate models, dynamical downscaling and hydrological modelling. Climate research, 16(2), 101-112 (2001).
14. J. D. Klipsch, M. B. Hurst. "HEC-ResSim reservoir system simulation user's manual version 3.0." USACE, Davis, CA 512 (2007).
15. S. Bergström, V. P. Singh. The HBV Model. In: Singh VP (ed) Computer Models of Watershed Hydrology. Water Resources Publications (2012).
16. J. Seibert. Estimation of parameter uncertainty in the HBV model. Nordic Hydrology, 28, 247-262 (1997).
17. J. Seibert, M. Vis. Teaching hydrological modeling with a user-friendly catchment-runoff-model software package. Hydrology and Earth System Sciences, 16, 3315–3325 (2012).
18. K. Ichii, M. A. White, P. Votava, A. Michaelis, R. R. Nemani. Evaluation of snow models in terrestrial biosphere models using ground observation and satellite data: impact on terrestrial ecosystem processes. Hydrological Processes 22:347-355 (2008).
19. D. P. Turner, D. R. Conklin, K. B. Vache, C. Schwartz, A. W. Nolin, H. Chang, E. Watson, J. P. Bolte. Assessing mechanisms of climate change impact on the upland forest water balance of the Willamette River Basin, Oregon. Ecohydrology 16:2345-2355 (2016).
20. R. G. Allen, I. A. Walter, R. Elliot, T. Howell, D. Itenfisu, M. Jensen, Snyder R. The ASCE standardized reference evapotranspiration equation, Report 0-7844-0805-X, 59 pp.

21. P. G. Jarvis. The interpretation of the variations in leaf water potential and stomatal conductance found in canopies in the field. Philosophical Transactions Royal Society B 273:593-610 (1976).
22. F. M. Kelliher, R. Leuning, E. D. Schulze. Evaporation and canopy characteristics of coniferous forests and grasslands. Oecologia 95:153-163 (1993).
23. P. Grieu, J. M. Guehl, G. Aussenac. The effects of soil and atmospheric drought on photosynthesis and stomatal control of gas-exchange in 3 coniferous species. Physiologia Plantarum 73:97-104 (1988).
24. S. Wharton, M. Schroeder, K. Bible, M. Falk, K. T. Paw. Stand-level gas-exchange responses to seasonal drought in very young versus old Douglas-fir forests of the Pacific Northwest, USA. Tree Physiology 29:959-974 (2009).
25. B. J. Bond, K. L. Kavanagh. Stomatal behavior of four woody species in relation to leaf-specific hydraulic conductance and threshold water potential. Tree Physiology 19:503-510 (1999).
26. R. G. Allen, L.S. Pereira, D. Raes, M. Smith. Crop Evapotranspiration-Guidelines for Computing Crop Water Requirements-FAO Irrigation and Drainage Paper 56. FAO, Rome 300:6541 (1998).
27. R. G. Allen, C.W. Robison. Evapotranspiration and Consumptive Irrigation Water Requirements for Idaho. University of Idaho Research and Extension, Kimberly, Idaho (2007).
28. J. Seibert, HBV-Light. Stockholm. http://people.su.se/~jseib/HBV/HBV_light.html (2005).
29. V. Chow, D. Maidment, L. Mays. Applied Hydrology. (McGraw-Hill, New York, 1988).
30. N. A. Abebe, F. L. Ogden, N. R. Pradhan. Sensitivity and uncertainty analysis of the conceptual HBV rainfall-runoff model: Implications for parameter estimation. Journal of Hydrology 389: 301-310 (2010).
31. A. Aghakouchak, E. Habib. Application of a Conceptual Hydrologic Model in Teaching Hydrologic Processes. Int. J. Engng Ed. 26(4): 963-973 (2010).
32. A. M. Inouye. Development of a Hydrologic Model to Explore Impacts of Climate Change on Water Resources in the Big Wood Basin, Idaho. M.S. thesis (Oregon State University, 2015).
33. S. Steele-Dunne, P. Lynch, R. McGrath, T. Semmler, S. Wang, J. Hanafin, P. Nolan. The impacts of climate change on hydrology in Ireland. Journal of Hydrology 356: 28-45 (2008).
34. US Geological Survey (USGS). Land Cover Trends. http://landcovertrends.usgs.gov/. Updated (December 13, 2012; accessed Mar 10, 2013).
35. D. P. Bigelow. How do population growth, land-use regulations, and precipitation patterns affect water use? A fine-scale empirical analysis of landscape change. PhD Dissertation (Oregon State University, 2015).
36. J. A. Hausman, W.E. Taylor. Panel data and unobservable individual effects. Econometrica, 49(6): 1377-1398 (1981).
37. J. K. Abbott, H.A. Klaiber. An embarrassment of riches: Confronting omitted variable bias and multiscale capitalization in hedonic price models. The Review of Economics and Statistics, 93(4): 1331-1342 (2011).
38. Y. Mundlak. On the pooling of time series and cross section data. Econometrica, 46(1): 69-85 (1978).
39. J. M. Wooldridge. Selection corrections for panel data models under conditional mean independence assumptions. Journal of Econometrics, 68: 115-132 (1996).
40. J. M. Wooldridge. Introductory Econometrics: A Modern Approach. Second Edition. (Mason, Ohio: Southwestern, 2003).

41. D. J. Lewis, A. J. Plantinga, E. Nelson, S. Polasky. The efficiency of voluntary incentive policies for preventing biodiversity loss. Resource and Energy Economics, 33: 192-211 (2011).
42. R. N. Lubowski, A. J. Plantinga, R.N. Stavins. Land-use change and carbon sinks: Econometric estimation of the carbon sequestration supply function. Journal of Environmental Economics and Management, 51: 135-152 (2006).
43. Dempsey, J.A., and A.J. Plantinga. How well do urban growth boundaries contain development? Results for Oregon using a difference-in-difference estimator. *Regional Science and Urban Economics,* 43(6): 997-1007 (2013).
44. Loveland, T.R., T.L. Sohl, S.V. Stehman, A.L. Gallant, K.L. Sayler, and D.E. Napton. A strategy for estimating the rates of recent United States land-cover changes. *Photogrammetric Engineering and Remote Sensing,* 68(10): 1091-1099 (2002).
45. D. P. Turner, D. R. Conklin, J. P. Bolte. Projected climate change impacts on forest land cover and land use over the Willamette River Basin, Oregon, USA. Climatic Change 133:335-348 (2015).
46. B. M. Rogers, R. P. Neilson, R. Drapek, J. M. Lenihan, J. R. Wells, D. Bachelet, B. E. Law. Impacts of climate change on fire regimes and carbon stocks of the U.S. Pacific Northwest. Journal of Geophysical Research-Biogeosciences 116:13 (2011).
47. D. P. Turner, D. Ritts, R. E. Kennedy, A. Gray, Z. Yang. Effects of harvest, fire, and pest/pathogen disturbances on the West Cascades ecoregion carbon balance. Carbon Balance and Management 10:12 (2015).
48. Sheehan T, Bachelet DB, Ferschweiler K. Projected major fire and vegetation changes in the Pacific Northwest of the conterminous United States under selected CMIP5 climate futures. Ecological Modelling 317:16-29 (2015).
49. P. E. Thornton, B. E. Law, H. L. Gholz, K. L. Clark, E. Falge, D. S. Ellsworth, A. H. Goldstein, R. K. Monson, D. Hollinger, M. Falk, J. Chen, J. P. Sparks. Modeling and measuring the effects of disturbance history and climate on carbon and water budgets in evergreen needleleaf forests. Agricultural and Forest Meteorology 113:185-222 (2002).
50. D. P. Turner, W. D. Ritts, Z. Q. Yang, R. E. Kennedy, W. B. Cohen, M. V. Duane, P. E. Thornton, B. E. Law. Decadal trends in net ecosystem production and net ecosystem carbon balance for a regional socioecological system. Forest Ecology and Management 262:1318-1325 (2011).
51. ORNL. Oak Ridge National Laboratory. http://daac.ornl.gov/DAYMET/guides/Daymet_mosaics.html#Daymet_m_citation (2014).
52. J. D. Marshall, R. H. Waring. Comparison of methods of estimating leaf-area index in old-growth Douglas-fir. Ecology 67:975-979 (1986).
53. FIA. U.S. Department of Agriculture Forest Inventory and Analysis Program, http://fia.fs.fed.us (2006).
54. D. Getches, S. Zellmer, A. Amos. *Water Law in a Nutshell, 5th*. (West Academic 2015).80.
55. A. Amos. "Freshwater Conservation in the Context of Energy and Climate Policy: Assessing Progress and Identifying Challenges in Oregon and the Western United States." U. Denv. Water L. Rev. 12: 1 (2008).
56. NMFS. 2008-2023 Willamette River Basin Project Biological Opinion. NOAA's National Marine Fisheries Service, Northwest Region, Seattle, WA. F/NWR/2000/02117 (2008).
57. USACE. HEC-ResSim Reservoir System Simulation: User's Manual, Version 3.1 (http://www.hec.usace.army.mil/software/hec-ressim/) (2013).

58. S. M. Olmstead, W. M. Hanemann, R.N. Stavins. Water Demand Under Alternative Price Structures. Journal of Environmental Economics and Management 54: 181-198 (2007).
59. S. M. Olmstead. Reduced-Form vs. Structural Models of Water Demand Under Non-Linear Prices. Journal of Business and Economic Statistics 27(1): 84-94 (2009).
60. S. M. Olmstead. The Economics of Managing Scarce Water Resources. Review of Environmental Economics and Policy 4(2): 179-198 (2010).
61. D. R. Bell, R. C. Griffin. Urban Water Demand with Periodic Error Correction. Land Economics 87(3): 528 – 544 (2011).
62. E. T. Mansur, S. M. Olmstead. The Value of Scarce Water: Measuring the Inefficiency of Municipal Regulations. Journal of Urban Economics 71: 332-346 (2012).
63. Portland Water Bureau. Water Management and Conservation Plan (2010).
64. S. Gaudin. Effect of Price Information on Residential Water Demand. Applied Economics 38: 383-393 (2006).
65. Environmental Protection Agency (EPA). 2006 Community Water System Survey (2009).
66. Portland Water Bureau. Conservation Rate Structure Review (June 2013).
67. Corvallis Water Management and Conservation Plan (November 2012).
68. Salem Water Management and Conservation Plan Final Report (March 2009).
69. Eugene Water Management and Conservation Plan (January 2012).
70. Springfield Utility Board. http://www.subutil.com/. Accessed 2012. .
71. A. Kalinin. Right as Rain?: The Value of Water in Willamette Valley Agriculture. Oregon State University, Corvallis, OR (2013).
72. R. Mendelsohn, W. D. Nordhaus, D. Shaw. “The Impact of Global Warming on Agriculture: A Ricardian Analysis.” The American Economic Review 84(4): 753-771 (1994).
73. G. Fipps. Calculating Horsepower Requirements and Sizing Irrigation Supply Pipelines. Texas Agricultural Extension Service, B-6011, Texas A&M University (1995).
74. M. English. Irrigation and Pumping. Manuscript, unpublished (2015).

Table S1. WRB population by county, 2010 with projections to 2100

County	2010	2020	2030	2040	2050	2060	2070	2080	2090	2100
Benton	85,735	91,379	98,516	105,050	111,666	117,965	124,654	131,324	138,046	144,747
Clackamas	376,780	422,576	485,054	537,753	583,814	632,743	683,634	733,473	784,317	835,025
Columbia	49,430	54,517	61,273	66,683	71,406	76,602	81,893	87,075	92,382	97,665
Lane	352,010	378,335	410,247	437,345	464,839	484,993	510,123	535,347	561,186	586,691
Linn	116,840	128,454	143,673	156,505	168,189	182,975	196,074	208,984	222,121	235,208
Marion	315,900	355,189	406,612	453,557	498,624	546,985	594,121	640,937	688,158	735,286
Multnomah	736,785	807,198	879,987	936,729	982,504	1,043,468	1,099,046	1,153,091	1,208,765	1,264,178
Polk	75,495	88,081	105,274	121,044	135,877	151,482	167,094	182,557	198,156	213,739
Washington	531,070	622,368	731,125	830,100	915,979	1,029,672	1,129,306	1,227,089	1,326,142	1,425,214
Yamhill	99,405	113,611	133,907	151,564	167,300	185,049	202,225	219,098	236,251	253,371

Table S2. Mean household total personal income by county, 2010 with projections to 2010

	2010	2020	2030	2040	2050	2060	2070	2080	2090	2100
Benton	81,135	90,837	111,158	138,697	159,685	183,327	207,001	230,198	253,719	277,111
Clackamas	106,818	115,168	135,842	164,259	185,514	209,709	233,902	257,593	281,633	305,531
Columbia	80,447	87,493	100,768	118,270	131,802	146,987	162,141	177,027	192,106	207,105
Lane	73,652	78,525	92,866	112,348	126,928	143,555	160,150	176,421	192,924	209,330
Linn	70,689	76,486	89,999	107,938	121,658	137,143	152,595	167,768	183,141	198,431
Marion	83,378	89,362	105,957	128,319	145,205	164,373	183,508	202,279	221,311	240,233
Multnomah	86,976	94,535	112,009	134,985	152,595	172,482	192,297	211,771	231,498	251,115
Polk	75,922	78,801	90,878	107,493	119,668	133,724	147,728	161,453	175,383	189,224
Washington	96,366	96,077	109,461	130,367	144,147	160,894	177,606	193,837	210,410	226,841
Yamhill	83,544	89,774	105,060	125,919	141,576	159,383	177,173	194,605	212,289	229,870

S3. Normalized root-mean-square-error of observed flows (reservoir inflows) vs. modeled inflows, 1980-2009

Tributary/reservoir	Annual	Nov-May	Jun-Oct
Blue River Lake	41%	33%	65%
Cottage Grove Lake	24%	19%	63%
Cougar Reservoir	22%	19%	27%
Detroit Lake	16%	15%	19%
Dorena Lake	27%	22%	44%
Fall Creek Lake	34%	28%	52%
Fern Ridge Lake	31%	24%	122%
Green Peter Lake	24%	20%	34%
Hills Creek Lake	15%	14%	13%

Table S4. Calibration parameter values by subbasin

Basin	Subbasin	CFMAX	CFR	FC	BETA	PERC	UZL	K0	K1	K2
Willamette mainstem	Lower mainstem	6.00	0.069	536	4.83	0.20	30.85	0.27	0.15	0.00
Middle Fork Willamette	Hills Creek Reservoir drainage	3.74	0.001	151	1.38	0.20	7.27	0.49	0.13	0.01
Middle Fork Willamette	Fall Creek Reservoir drainage	3.28	0.080	201	1.35	0.18	0.96	0.55	0.25	0.01
Coast Fork Willamette	Dorena Reservoir drainage	2.74	0.026	280	1.24	0.19	1.11	0.59	0.29	0.03
Coast Fork Willamette	Cottage Grove Reservoir drainage	2.98	0.054	521	1.02	0.16	8.50	0.22	0.15	0.04
Long Tom River	Fern Ridge Reservoir drainage	4.67	0.034	392	2.50	0.20	2.09	0.59	0.29	0.01
McKenzie River	Cougar Reservoir drainage	2.64	0.014	330	1.11	0.20	9.13	0.57	0.23	0.03
McKenzie River	Blue River Reservoir drainage	2.53	0.054	220	1.15	0.19	4.43	0.59	0.26	0.03
South Santiam River	Green Peter Reservoir drainage	4.06	0.010	191	2.24	0.19	1.37	0.53	0.28	0.06
North Santiam River	Detroit Reservoir drainage	3.45	0.009	148	1.14	0.20	8.89	0.60	0.29	0.01
Clackamas River	Above the River Mill gage	2.52	0.014	216	1.24	0.19	8.86	0.59	0.24	0.00
Willamette mainstem	Above the Salem gage	6.00	0.069	536	4.83	0.20	30.85	0.27	0.15	0.00
McKenzie River	Above the Walterville gage	2.98	0.047	225	4.50	0.20	8.17	0.57	0.08	0.00
Long Tom River	Above the Monroe gage	4.67	0.034	392	2.50	0.20	2.09	0.59	0.29	0.01
South Santiam River	Above the Waterloo gage	4.06	0.010	191	2.24	0.19	1.37	0.53	0.28	0.06
North Santiam River	Above the Mehama gage	3.45	0.009	148	1.14	0.20	8.89	0.60	0.29	0.01
Middle Fork Willamette	Above the Jasper gage	3.28	0.080	201	1.35	0.18	0.96	0.55	0.25	0.01
Coast Fork Willamette	Above the Goshen gage	6.00	0.069	536	4.83	0.20	30.85	0.27	0.15	0.00
Tualatin River	Above the West Linn gage	5.77	0.026	271	3.08	0.18	0.21	0.60	0.30	0.00
Yamhill River	Above the McMinnville gage	5.77	0.026	271	3.08	0.18	0.21	0.60	0.30	0.00
Lower bound:		2.50	0	50	1.00	0.01	0	0.10	0.01	0
Upper bound:		6.00	0.100	550	6.00	0.20	80.00	0.60	0.30	0.10

Table S5. Variable descriptions and sources for hedonic land value models.

Variable	Description	Source
Constant	Constant term: applies to all observations, includes effects of year 2000 dummy variable and average lot size for developed sample parcels (0.39 acres)	County assessment offices (lot size)
UGB	Equals 1 if parcel located within UGB; 0 otherwise	Dept. of Land Conservation and Development
Population density	Population density of nearest UGB for a city with a population of greater than 20,000 (people per acre)	US Census of Population
Household income	Natural log of household income in county where parcel is located ($ thousands)	Woods and Poole
Improvement value	Value of improvements on parcel	County assessment offices
Distance to city center	Euclidean distance to nearest city center (in miles; cities defined as those with population >20,000)	Google Maps (used for generating city centroid)
Distance to city center^2	Squared Euclidean distance to nearest city center	Google Maps (used for generating city centroid)
Benton County	Equals 1 if parcel located in Benton County group; 0 otherwise	County assessment offices
Lane County	Equals 1 if parcel located in Lane County group; 0 otherwise	County assessment offices
Washington County	Equals 1 if parcel located in Washington County group; 0 otherwise	County assessment offices
Acres	Acreage of parcel	County assessment offices
Slope	Average slope of parcel (degrees)	US Geological Survey
Farmland rent	Farmland rental value ($/acre)	WW2100 Farmland Rent model (see Section S5.4.3)
Improvement value	Mean improvement value over sample years ($/acre)	County assessment offices
Elevation	Elevation of parcel (feet)	US Geological Survey
River footage	Footage of rivers and streams running through parcel	Environmental Protection Agency
Private non-industrial owner	Equals 1 if under private non-industrial ownership; 0 otherwise	Oregon State Forestry Science Lab
Distance to UGB	Distance to nearest UGB boundary	Department of Land Conservation and Development

Table S6. Hedonic land value model coefficients.

	Agriculture	Urban	Forest
Year1980	-0.260***	0.676***	0.119*
	(-5.750)	(16.90)	(1.87)
Year1986	-0.942***	0.569***	-0.438***
	(-15.91)	(13.61)	(-5.290)
Year1992	-1.066***	0.526***	-0.455***
	(-13.49)	(11.61)	(-4.421)
Year2000	0.516***	1.269***	0.0321
	(3.54)	(19.05)	(0.19)
Parcel size (acres)	-0.00768***	-0.518***	-0.000335
	(-6.286)	(-29.38)	(-1.383)
Benton County	-0.209*	0.0923**	-0.996***
	(-1.797)	(2.14)	(-8.949)
Lane County	-0.354***	-0.276***	-0.295***
	(-3.738)	(-7.972)	(-2.769)
Washington County	-0.786***	0.239***	-1.274***
	(-3.915)	(6.12)	(-7.157)
Distance to urban center	-0.0182	-0.0458***	-0.111***
	(-1.193)	(-8.354)	(-7.928)
Distance to urban center (squared)	0.000459	0.000765***	0.00187***
	(1.11)	(6.90)	(6.56)
Population density	0.179***	0.107***	0.137**
	(3.52)	(9.35)	(2.41)
Household income	0.0335***	0.627***	0.0590***
	(8.73)	(5.59)	(11.06)
Inverse Mill's ratio	-0.335**	0.130***	0.205
	(-2.460)	(4.10)	(1.53)
Improvement value	0.000975**	0.00106***	0.000333
	(2.55)	(13.20)	(1.42)

Table S6. WW2100 hedonic model coefficients (continued).

	Agriculture	Urban	Forest
UGB*Year1980		0.0529	
		(1.30)	
UGB*Year1986		-0.147***	
		(-3.647)	
UGB*Year1992		-0.218***	
		(-5.445)	
UGB*Year2000		-0.322***	
		(-7.953)	
UGB		0.756***	
		(12.84)	
Slope (degrees)	-0.0144		-0.0514***
	(-1.195)		(-8.536)
Farmland rent	0.00264**		
	(2.42)		
Elevation			-0.00105***
			(-4.431)
River footage			-8.97e-05**
			(-2.328)
Private non-industrial owner			0.252***
			(3.35)
Zoned for agriculture or forest	-0.345***		-0.672***
	(-3.419)		(-6.417)
UGB distance	-0.0312**		0.0393***
	(-1.988)		(3.20)
Mean population density	-0.115		
	(-1.377)		
Mean household income	-0.0163		-0.0148**
	(-1.582)		(-1.982)
Mean inverse Mill's ratio	1.027***		0.894***
	(2.76)		(3.00)
Mean improvement value	0.00204*		0.00588***
	(1.68)		(7.06)
Constant	6.994***	7.606***	5.849***
	(13.50)	(17.16)	(12.61)
Correction factor	1.167	1.035	1.226
Observations	4,392	8,640	3,753
Observations	1,056	2,735	948

Note: t-statistics in parentheses; significance levels: * $p < 0.1$, ** $p < 0.05$, *** $p < 0.01$.

Table S7. Potential land conversions.

		Ending use:		
		Agriculture	Forest	Developed
Starting use:	Agriculture	P_{aa}	P_{af}	P_{ad}
	Forest	P_{fa}	P_{ff}	P_{fd}

Table S8. Economic returns scaling formulas.

	Returns to:	Agriculture	Forest	Development
Starting use:	Agriculture	Min(Max(0,ag_val*0.05),200)	Min(Max(0,for_val*1.6),2000)	Min(Max(0,dev_val),7500)
	Forest	Min(Max(0,ag_val*0.01),2000)	Min(Max(0,for_val*0.7),200)	Min(Max(0,dev_val),7500)

Table S9. Land-use model validation: Comparison of projected land development rates from WW2100 (2010-2100) to historical rates of change (1973-2000).

	WW2100 model overall 1/	WW2100 model results scaled to fit the Land Cover Trends Willamette Valley ecoregion 2/	Land Cover Trends Willamette Valley ecoregion data 3/
Time period (years)	2010-2100	2010-2100	1973-2000
From agriculture to development			
initial use area (acres)	1,563,274	1,542,706	1,683,480
area change (acres)	122,552	122,378	85,745
% change based on initial area	7.84	7.93	5.09
% of study area that changed from ag to dev	1.71	3.88	2.4
From forest to development			
initial use area (acres)	5,048,995	1,115,074	1,383,494
area change (acres)	57,957	53,940	25,452
% change based on initial area	1.15	4.84	1.84
% of study area that changed from for to dev	0.81	1.71	0.80
Base area (acres)	7,154,591	3,157,073	3,421,596

1/ The overall WW2100 land-use changes were developed by summing the acreage of the WW2100 individual decision units (IDUs) that started in agriculture or forest and ended in development.

2/ The refined WW2100 land-use changes were developed by summing the acreage of the IDUs that started in agriculture or forest and ended in development, after removing all IDUs that fall outside of the Willamette Valley ecoregion (as measured in the LCT data). Approximately 98% of all developed land in the WW2100 project is contained in the WV ecoregion.

3/ The LCT data cover the Willamette Valley. The vast majority of the WV falls in Oregon, but a small portion covers the Vancouver, WA metro area. The forest-development category includes land that was originally classified as mechanically disturbed, as this often signifies clearcutting. These estimates were taken from the U.S. Geological Survey's Land Cover Trends website: https://landcovertrends.usgs.gov/west/eco3Report.html.

Other notes

LCT - Overall change indicate 3.1% increase in development, 2.2% decrease in agriculture, 4.1% decrease in forest, 2.8% increase in mechanically disturbed, 0.4% increase in grassland

WW2100 area overlapping with LCT WV - 3157073.18497 acres (developed: 331184.281825 acres in 2010, 507501.689331 acres in 2100)

WW2100 area - 7154591.078225 acres (developed: 335543.077413 acres in 2010, 516052.514647 acres in 2100)

About 98% of all developed land in WW2100 is in LCT WV ecoregion

Table S10. Reservoir zones in ResSim Lite model

Zone	Description
Top of dam	Where overtopping would occur.
Flood control	Max pool available for flood regulation.
Conservation	The “Rule Curve” which includes minimum and maximum conservation pools.
Buffer	Acts like an interim draft limit to keep pool from drafting too low below minimum conservation pool.
Inactive	The lowest pool that can access outlets.

Table S11. Operating rule types

Rule type
Minimum
Maximum
Increasing rate
Decreasing rate
Control point
Power plant rule (gate specific)
Regulating outlet rule (gate specific)
Spillway rule (gate specific)

Table S12. Biological Opinion minimum flow objectives for Willamette River at Salem.

Time period	Weekly average minimum flow (cubic feet per second)	Instantaneous minimum flow (cubic feet per second)
April 1-15	17,800	14,300
April 16-30	17,800	14,300
May 1-21	15,000	12,000
June 1-15	13,000	10,500
June 16-30	8,700	7,000

Source *(52)*

Table S13. Congressionally authorized minimum flow objectives, Willamette River at Salem and Albany.

Time period	Average flow at Albany (cfs)	Average flow at Salem (cfs)
June 1-30	4,500	N/A
July 1-31	4,500	6,000
August 1-15	5,000	6,000
August 16-31	5,000	6,500
September 1-30	5,000	7,000
October 1-31	5,000	7,000

Source *(52)*

Table S14. Water year types based on total volume stored in all federal reservoirs (million acre-feet).

Water Year Types	Abundant	Adequate	Insufficient	Deficit
May 20th storage:	≥ 1.48	1.20 to 1.47	0.90 to 1.19	< 0.90

Table S15. Estimated and reported water use for major municipalities in the Willamette Basin

Urban Area	Predicted water use for 2010 in gallons per capita per day	Reported water use in gallons per capita per day (year)
Portland Metro	108	111 (2011)
Corvallis	124	129 (2009)
Salem - Keizer	122	124 (2007)*
Eugene - Springfield	118	Eugene: 144 (2009) Springfield: 129 (2010)
Average	112	124

Sources, in order by row *(62,63,64,(65 and 66)).* * For Salem only.

Table S16. City of Portland: water prices, actual water use and predicted use based on WW2100 model (gal./person/day).

Year	Water price (2010 $/ccf)	Actual water use	Predicted water use
1995	1.35	150	127
1996	1.36	144	127
1997	1.35	143	128
1998	1.34	144	130
1999	1.37	140	129
2000	1.88	142	107
2001	1.85	134	108
2002	1.80	134	109
2003	1.90	135	106
2004	2.02	133	102
2005	2.00	124	103
2006	2.01	129	103
2007	2.02	130	106
2008	2.00	125	106
2009	2.20	123	100
2010	2.55	119	92
2011	2.80	111	87

Sources: for actual water use 1995-2005 *(59)*, growth rates from 2006-2011 and for prices *(62)*.

Table S17. Crop choice model parameter estimates

Coefficient	Grass seed	Pasture	Wheat	Fallow	Corn	Clover	Hay
β_0	0.2220***	0.3702***	0.0126	0.066***	-0.0041	0.0154***	0.0616***
β_1	0.1656***	-0.1870***	0.0655***	-0.0340***	0.0076	-0.0031	-0.0613***
β_2	0.1545***	-0.1793***	0.0535***	-0.0309***	0.0147	0.0079	-0.0576***
β_3	0.1453***	-0.1237***	0.0294*	-0.0315***	0.0183	0.0024	-0.0411***
β_4	0.2361***	-0.0546	0.0135	-0.0349***	0.0045	-0.0036	-0.0528***
β_5	-0.2460***	-0.2004***	-0.0054	-0.0191	0.1213***	-0.0044	-0.0369*
β_6	0.1030 **	-0.0503	0.0111	-0.0127	0.0123	-0.0103	-0.0472***
β_7	-0.2976***	-0.1071	0.0511	0.0419	0.0541**	-0.011	-0.0329*
β_8	-0.0006***	0.0007***	-0.0001**	0.0005***	-0.0002***	0.000002***	-0.0001***
β_9	-0.0169***	0.0071***	-0.0002	0.0033***	-0.0010***	-0.0002	0.0007***
β_{10}	-0.0133***	0.0218***	-0.0067***	0.0054***	0.0027***	-0.0035***	-0.0001
β_{11}	-0.0500***	-0.0358***	0.0042**	-0.0084***	-0.0059	0.0088***	-0.0001***
β_{12}	0.0092***	-0.0160***	-0.0026***	0.0080***	0.0003***	-0.0002***	0.0004***
β_{13}	-0.0147***	0.0745***	0.0020**	-0.0125***	-0.0041***	-0.0024***	-0.0170***
β_{14}	-0.0591***	-0.0262***	-0.0047***	0.001	0.0185***	-0.0078***	-0.0016**

Note: significance levels indicated as: * $p < 0.1$, ** $p < 0.05$, *** $p < 0.01$.

Table S18. Irrigation decision model parameter estimates.

Variables	Coefficient	P-Value
June precipitation (deviation from mean)	-0.0943*	0.065
July precipitation (deviation from mean)	-0.4134**	0.005
August precipitation (deviation from mean)	-0.1584	0.188
Elevation	-0.0098***	0.000
Elevation*(precipitation April-June)	0.0008***	0.000
EFU (Exclusive farm use) zoning	0.4307***	0.000
Field size (acres)	-0.0038***	0.000
Groundwater irrigation water right	0.3311***	0.000
Poorly drained soils (%)	-0.0084***	0.000
Groundwater right*depth	-0.0094***	0.000
Water holding capacity	-0.2190***	0.000
Distance to Willamette River	-0.0261***	0.000
Distance to large city	-0.0087**	0.037
Soil type LCC1	0.8397***	0.002
Soil type LCC2	1.0799***	0.000
Soil type LCC3	0.8206***	0.001
Soil type LCC4	1.4981***	0.000
Constant	2.42***	0.000

Note: significance levels indicated as: * $p < 0.1$, ** $p < 0.05$, *** $p < 0.01$.

Table S19. Farmland rent model parameter estimates.

Variables	Coefficient		P-values
Soil LCC 1 (unirrigable)	104.7	***	0.0000
Soil LCC 2 (unirrigable)	95.6	***	0.0000
Soil LCC 3 (unirrigable)	69.9	***	0.0000
Soil LCC 4 (unirrigable)	66.6	***	0.0000
Soil LCC 6 (unirrigable)	20.5	***	0.0000
Soil LCC 7 (unirrigable)	19.9	***	0.0000
Soil LCC 1 (irrigable)	143.6	***	0.0000
Soil LCC2 (irrigable)	134.7	***	0.0000
Soil LCC3 (irrigable)	87.7	***	0.0000
Soil LCC4 (irrigable)	88.7	***	0.0000
Elevation (demeaned)	-1.06	***	0.0070
Precipitation (demeaned)	98.5	***	0.0000
Temperature min (demeaned)	351.6	***	0.0000
Elevation*Acres	-0.02	***	0.0000
Precipitation*Acres	-0.44	***	0.0000
Temperature*Acres	20.1	***	0.0000
Constant	65.5	***	0.0000

Note: significance levels indicated as: * $p < 0.1$, ** $p < 0.05$, *** $p < 0.01$.

Table S20. Comparison of WW2100 model results and USDA Census of Agriculture.

Model results, reference scenario, 2010–2015			USDA Census of Agriculture, 2012	
Crop category	Harvested acres	Irrigated acres	Crop category	Harvested acres
Grass and clover seeds	350,067	101,870	Grass, clover, and other field seed crops	389,000
Hay and pasture	184,571	36,506		149,784
Orchards, vineyards, and tree farms	36,101	7,444	Orchards, vineyards, tree farms	74,893
Corn	13,468	8,304	Corn	38,765
Wheat	31,416	—	Wheat	97,700
Other crops	309,224	110,536	Other crops	161,641
Total	924,847			911,783
Total irrigated		264,600		267,000[1]

[1] Total irrigated acres is an average for Census of Agriculture 1997, 2002, 2007, 2012.

Table S21. Estimated mainline capital costs for new irrigation conveyance piping, for a range of representative systems.[1]

Pipe diameter (inches)	Cost ($/foot)	Capacity (gall./min)	Friction loss (psi)	Distance (feet)	Friction loss per 1,000 ft	Irrigable area (acres)		Cost per 100 feet conveyance ($/ac)		Annualized cost (per 100 feet) ($/acre)[2]		Annualized cost (per 100 meters)($/ac)[2]	
						7 gpm	6 gpm	7 gpm	6 gpm	7 gpm	6 gpm	7 gpm	6 gpm
10	17	1225	9.0	3000	3.0	175	204	9.7	8.3	$0.71	$0.61	$2.34	$2.01
8	9.5	780	9.6	2500	3.8	111	130	8.5	7.3	$0.63	$0.54	$2.06	$1.76
6	6.9	450	9.0	1600	5.6	64	75	10.7	9.2	$0.79	$0.68	$2.59	$2.22
5	5.8	305	9.3	1400	6.6	44	51	13.3	11.4	$0.98	$0.84	$3.21	$2.75
4	4.5	195	9.5	1100	8.6	28	33	16.2	13.8	$1.19	$1.02	$3.90	$3.34
3	4	110	9.1	750	12.1	16	18	25.5	21.8	$1.87	$1.61	$6.14	$5.27

[1/] Source for cost per foot, friction losses and irrigable areas, A. Knox, Pacific Ag Systems, Inc., Junction City, OR.

[2/] Costs are amortized over 20 years at 4%.

Table S22. Sensitivity of model metrics to scenario assumptions across 15 scenarios

	Standard deviation	Coefficient of variation	CV for subset of scenarios
Precip (mm H2O)	54.1	3.2%	
GW pumping (mm H2O)[a]	0.96	8.5%	4.0%
Water from outside the basin (mm H2O)[a]	1.41	18%	3.6%
Water to outside the basin (mm H2O)[b]	0.77	19%	3.7%
Recharge High Cascades aquifer (mm H2O)	0.40	2.0%	
Actual ET (mm H2O)	13.1	2.0%	
Snow evaporation (mm H2O)[c]	4.3	17%	1.6%
Basin discharge (mm H2O)	40.4	3.5%	
Total water in grondwater HRUs, streams, and reservoirs at end of this year (mm H2O)	8.48	1.4%	
Irrigation (ac-ft)[d]	38335	10%	2.0%
Municipal and rural water use (ac-ft)[b]	73736	17%	3.2%

a/ Subset of scenarios escluding two with high irrigation.

b/ Subset of scenarios excludes four with high population growth and one with zero growth.

c/ Subset excludes low and high climate scenarios.

d/ Subset excludes two "high irrigation" scenarios.

Note: The 15 scenarios include: the baseline or reference case, low climate change, high climate change, fire suppression, urban water full cost pricing, high population growth, zero population growth, zero income growth, permissive urban land expansion, low irrigation rates, high irrigation rates, new irrigation allowed, new instream regulated flows, and two extreme or worst case scenarios that combine multiples of these modifications. Details can be found at http://inr.oregonstate.edu/ww2100/data.

Figure S1. Soil water content: schematic of moisture stress coefficient, adapted from *(27)*.

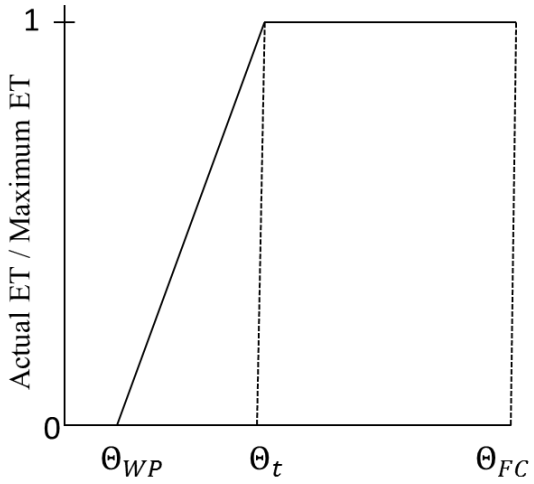

Figure S2. Hydrologic modeling within Willamette Envision involves movement of water through a set of conceptual reservoirs simulating soil and groundwater.

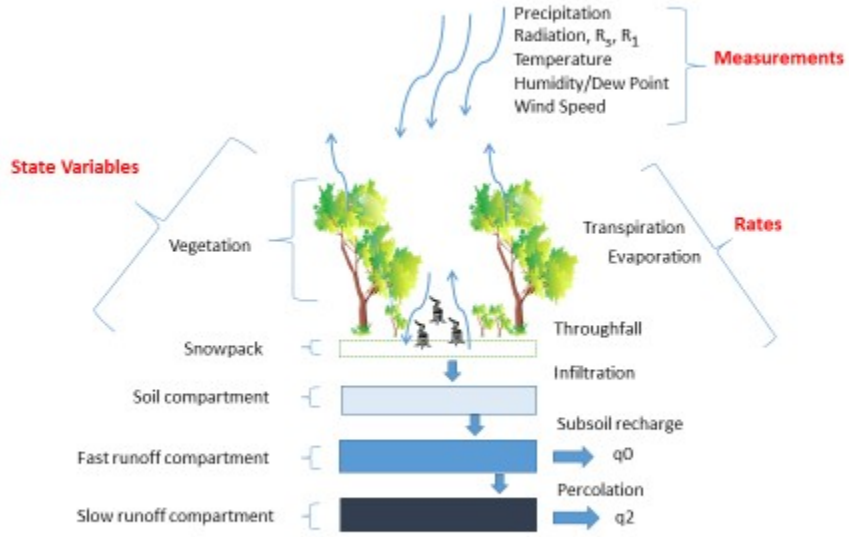

Figure S3. Locations and estimated marginal value of irrigation water rights (actual or potential).

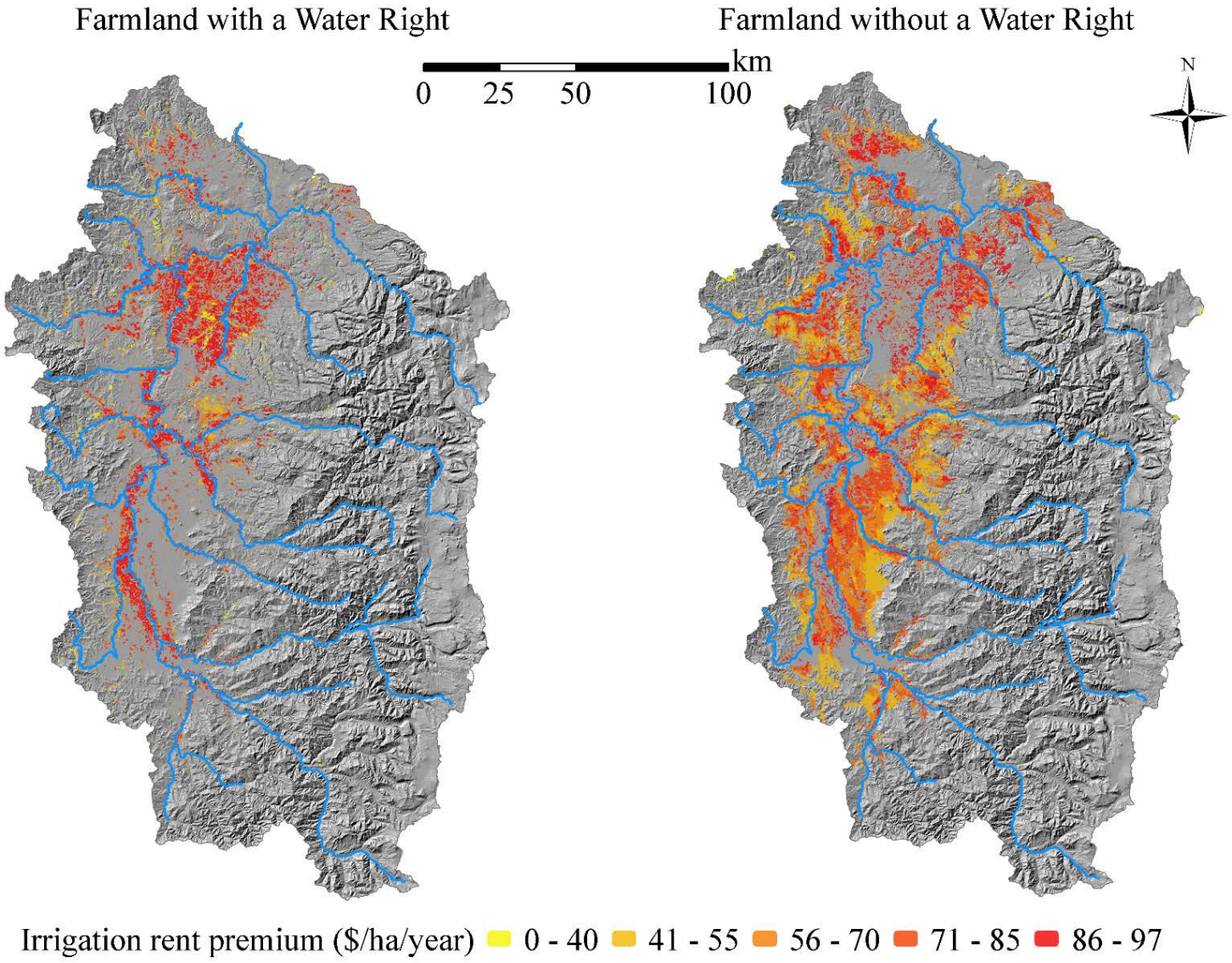

Figure S4. Reservoir operating zones (based on Lookout Point Reservoir).

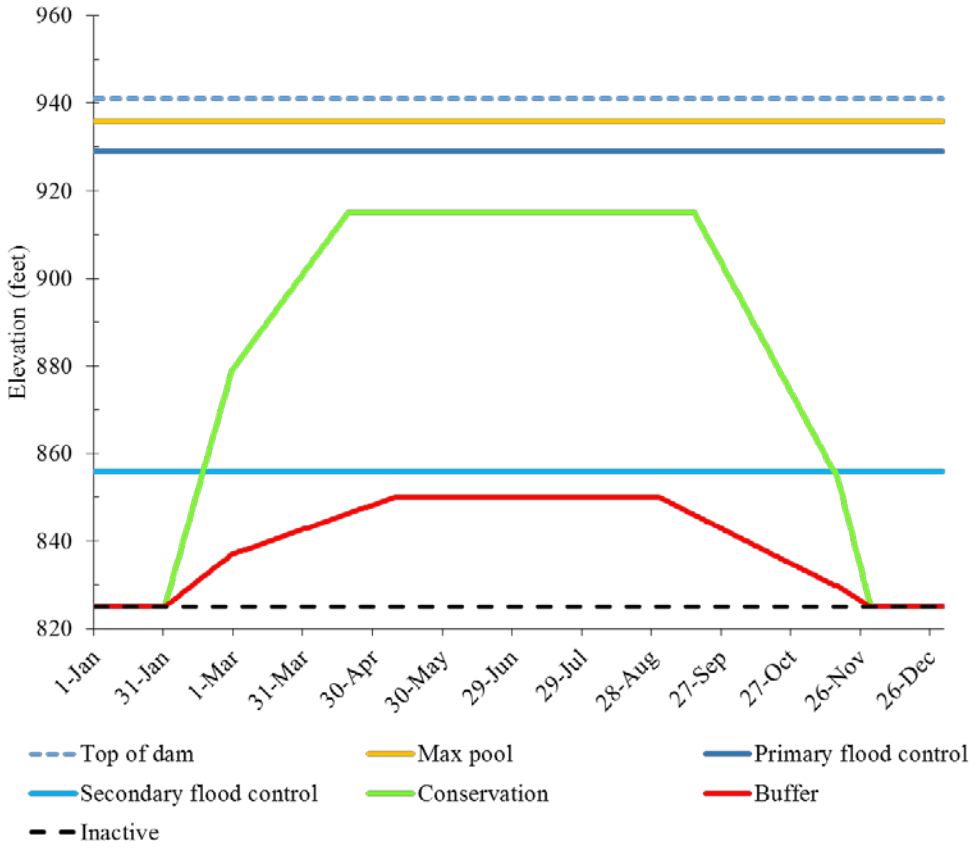

Notes: The conservation curve (green) is the primary rule curve. The zone above the rule curve is the Flood Control Zone, while below the curve is the Conservation Zone. If the pool elevation is above the elevation demarcating the primary flood control zone (horizontal dark blue line), the zone is labeled Top of Dam Zone. If the pool elevation falls below the red line, the zone is labeled the Buffer Zone. There also exists an alternative flood control zone in this case, when the pool elevation is above the rule curve but below the secondary flood control line (in light blue).

Figure S5. Portland water use – actual versus predicted

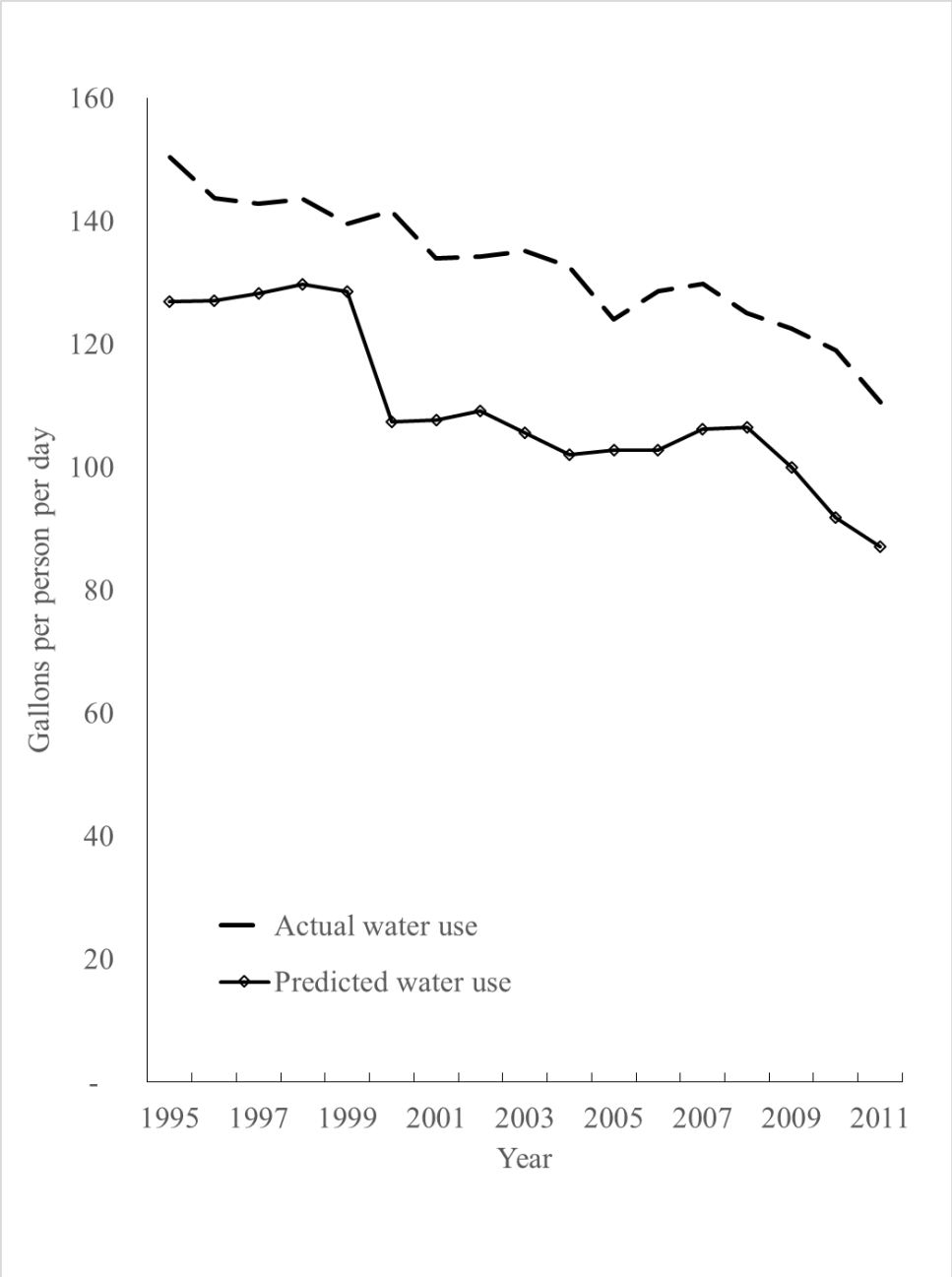

Figure S6. Scenario Descriptions

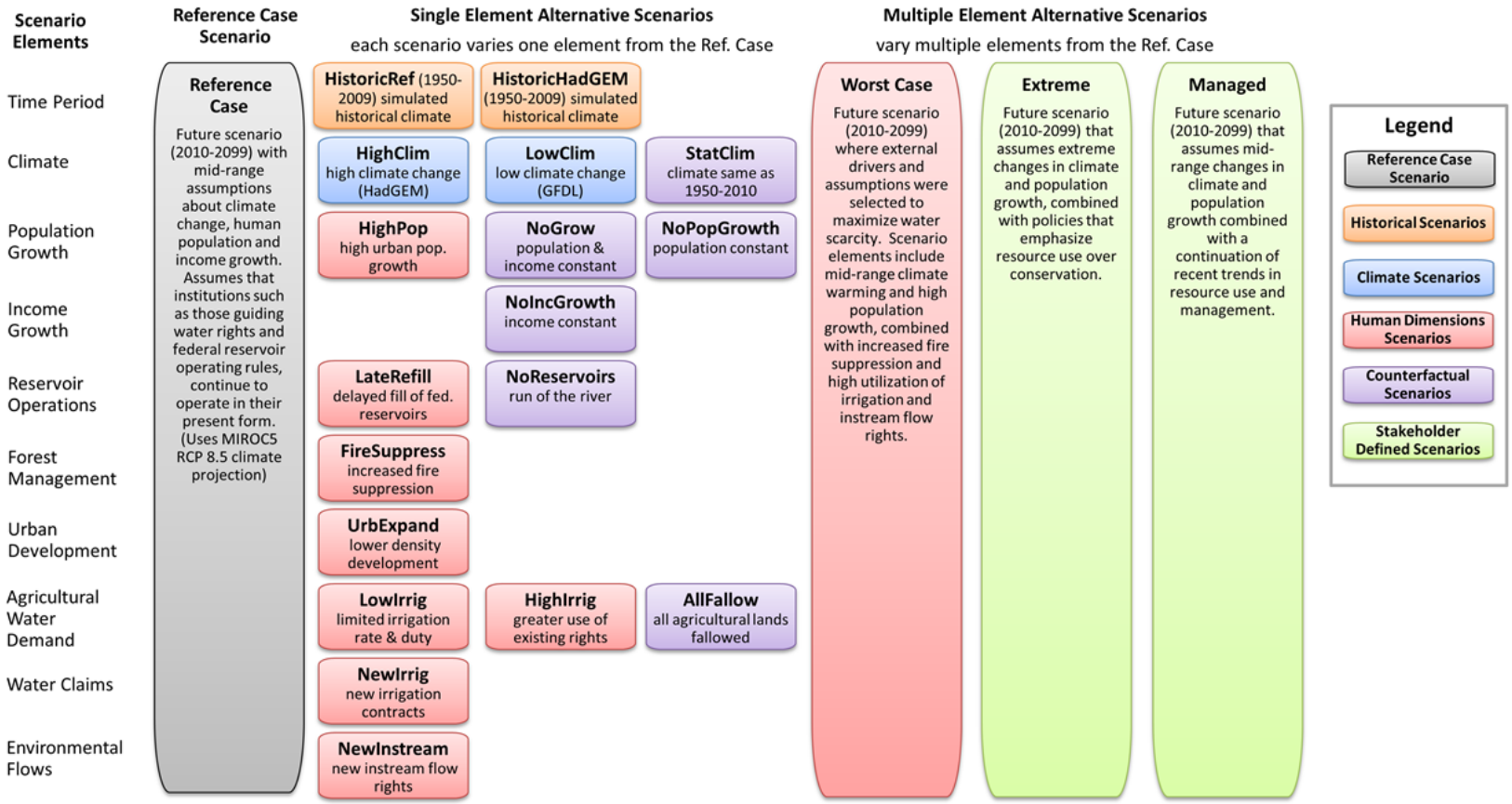

Details for each scenario are found at http://inr.oregonstate.edu/ww2100/data.